[redacted]

Copy 292
RM H57C25

NACA RM H57C25

DECLASSIFIED- US: 1688
AUTHORITY- TAINE TO
ROBERTSON MEMO DATED 9/28/66

NACA

Declassified by authority of NASA
Classification Change Notices No. 80
Dated ** 10/12/66

RESEARCH MEMORANDUM

CASE FILE COPY

ANALYSIS OF FLIGHT-DETERMINED AND PREDICTED EFFECTS OF FLEXIBILITY ON THE STEADY-STATE WING LOADS OF THE B-52 AIRPLANE

By Albert E. Kuhl, John T. Rogers, and Mary V. Little

High-Speed Flight Station
Edwards, Calif.

[redacted]

[redacted]

NATIONAL ADVISORY COMMITTEE
FOR AERONAUTICS

WASHINGTON
April 23, 1958

[redacted]

 DECL[redacted]IED

NATIONAL ADVISORY COMMITTEE FOR AERONAUTICS

RESEARCH MEMORANDUM

ANALYSIS OF FLIGHT-DETERMINED AND PREDICTED EFFECTS OF FLEXIBILITY ON THE STEADY-STATE WING LOADS OF THE B-52 AIRPLANE

By Albert E. Kuhl, John T. Rogers, and Mary V. Little

SUMMARY

To substantiate at low transonic speeds predicted effects of flexibility on the steady-state wing loads of large flexible airplanes employing sweptback wings, an investigation of the steady-state wing loads was conducted on the Boeing B-52 airplane. The investigation was conducted at speeds up to a Mach number of 0.82 at an altitude of 20,000 feet and up to a Mach number of 0.90 at 30,000 feet.

In general, the results of the investigation agreed with the trends that might be expected for a swept wing with high aspect ratio. The effect of wing bending rather than twist about the wing axis appeared to be predominant in changing the air-load distribution due to flexibility. Because the bending effect was predominant, the center of pressure moved inboard and forward with increasing dynamic pressure. The transonic rearward movement of the aerodynamic center started near a Mach number of 0.82 at a lift coefficient of 0.35 and occurred at progressively lower lifts with increasing Mach number until at the highest test Mach number of 0.90, the aerodynamic center remained in the rearmost position over the total lift region investigated.

The measured loads were compared with the results of calculations using the method of NACA TN 3030. The comparisons of the measured and calculated loads indicated that the method used to predict the loads appears reasonable for this type of airplane configuration in the speed range tested.

To illustrate the effects on the air loads of varying the structural properties, calculations were made in which the wing stiffness was varied. A 20-percent increase in wing stiffness resulted in generally small changes in the calculated shear, bending moment, and torque curves for the altitude and Mach number range of these tests. For a Mach number of 0.9 at an altitude of 30,000 feet a rigid-wing calculation showed an increase in

wing-root bending moment per unit normal-load factor of about 24.5 percent with a corresponding increase in root shear of about 7.5 percent.

Results of calculations in which the nacelle air loads were varied indicated that the nacelle air loads can have a strong influence on the total wing loads and therefore an accurate estimation of the nacelle air loads is important in predicting the wing loads.

INTRODUCTION

In recent years the role of airplane flexibility has assumed increasing importance in airplane design, particularly with jet bombers and transports where the trend is toward high-aspect-ratio sweptback wings. These high-aspect-ratio sweptback wings enable the designer to achieve greater airplane performance; however, these high-aspect-ratio surfaces and the increased speeds emphasize the aeroelastic problems resulting from airplane flexibility.

To substantiate the prediction of aeroelastic effects on a large flexible airplane capable of obtaining low transonic speeds, the National Advisory Committee for Aeronautics obtained flight-test data on the Boeing B-52 airplane. This program was completed through the cooperation of the U. S. Air Force and Boeing Airplane Co. The airplane used for this investigation was completely instrumented, maintained, and operated by the manufacturer. The NACA flight program was conducted by Boeing concurrently with the completion of the B-52 structural integrity program.

This paper presents the results obtained during the phase of the B-52 flight investigation concerned with the steady-state wing loads. Where possible, the effects of Mach number and flexibility on the measured loads are analyzed and presented. In addition, the measured and predicted loads are compared and the effects of varying some important aerodynamic and structural properties used in the predictions are also investigated. The parameters considered include the wing stiffness and the nacelle air loads.

SYMBOLS

b	wing span, in.
$\frac{b_w}{2}$	wing-panel semispan, in.
C_{N_A}	airplane normal-force coefficient, $\frac{nW}{qS}$

c local wing chord, in.

$\bar{c}$ wing mean aerodynamic chord, $\dfrac{\int_0^{b/2} c^2 dy}{\int_0^{b/2} c\, dy}$, in.

$\bar{c}_w$ wing-panel mean aerodynamic chord, $\dfrac{\int_{124.7}^{b/2} c^2 dy}{\int_{124.7}^{b/2} c\, dy}$, in.

c_{l_α} wing section lift-curve slope, per radian

EI wing bending stiffness, lb-sq in.

F_N wing shear, (positive for up load), lb

F_{N_0} wing shear at zero airplane normal acceleration, lb

GJ wing torsional stiffness, lb-sq in.

g acceleration of gravity, 32.2 ft/sec^2

h wing deflection, in.

h_p pressure altitude, ft

M Mach number

M_b wing bending moment, (positive if up load outboard of strain-gage station), in-lb

M_{b_0} wing bending moment at zero airplane normal acceleration, in-lb

n normal-load factor, g units

q free-stream dynamic pressure, lb/sq ft

S total wing area, sq ft

T wing torque about the wing elastic axis, (positive for up load ahead of elastic axis), in-lb

T_0 wing torque at zero airplane normal acceleration, in-lb

t time, sec

W airplane gross weight, lb

x_{ac} wing-panel aerodynamic center, percent $\bar{c}_w$

y lateral distance from airplane center line, in.

y_{cp_a} lateral center of pressure of additional air load, percent $\frac{b_w}{2}$

α_{BI} angle between root reference station geometric zero-lift line and the apparent zero-lift line at a particular wing spanwise location, including built-in twist and induced aerodynamic effects, radians

δ_e elevator angle, (positive when trailing edge of elevator down), deg

$\dot{\theta}$ pitching velocity, (positive when airplane pitching nose up), deg/sec

Λ angle of sweepback, deg

Subscripts:

cg center of gravity

N_1 inboard nacelle

N_2 outboard nacelle

T external wing tank

AIRPLANE

The Boeing RB-52 airplane used for this investigation is characterized by large flexible sweptback wing and tail surfaces. Two engine nacelles and an external fuel tank are mounted beneath each wing. The airplane employs hydraulically operated wing spoilers and a hydraulically operated adjustable stabilizer used for trim. In addition, the airplane has tab-operated ailerons, elevator, and rudder. A photograph and a three-view sketch of the airplane are shown in figures 1 and 2, respectively, and the pertinent physical characteristics are summarized in table I.

A camera was installed on the top of the fuselage for photographing wing, fuselage, and tail deflections.

The weight of the airplane during the flight tests was approximately 290,000 pounds and the center of gravity was maintained at 26 ±1 percent mean aerodynamic chord by transferring fuel within the body tanks. The fuel carried in the wings was held constant during these tests. The inboard wing tanks from station $\frac{2y}{b} = 0.11$ to $\frac{2y}{b} = 0.43$ were full. The outboard tanks and the external tank were empty.

INSTRUMENTATION

The instrumentation in the B-52 airplane was installed, calibrated, and maintained by the Boeing Airplane Co. The following measurements obtained during the flight tests are pertinent to the analysis presented:

- Airspeed and altitude
- Normal accelerations at center of gravity, tail, and three wing locations
- Elevator position
- Gross weight and center-of-gravity position
- Pitching velocity at center of gravity
- Wing loads
- Wing deflections

Wing shear, bending moment, and torque were measured by strain gages at the locations shown in figure 3. It should be noted that the measurements are relative to the assumed elastic axis (fig. 3). In addition to the six primary load stations, bending moment was also measured at nine other stations on the wing. The strain-gage zeros obtained on the ground prior to each flight were used to establish the load levels. The loads have been corrected for the wing and fuel dead-weight inertias and therefore are presented as aerodynamic loads acting on the wing.

Wing deflections were measured at eight locations on each wing panel. The target locations used to measure the deflection of the left wing are shown in figure 3. The camera used to photograph the targets was mounted over the wing center section as shown in the three-view drawing (fig. 2). The camera housing was the only external change made to the B-52 configuration.

The estimated accuracy of the measured quantities is ±3 percent.

TESTS

The flight tests reported in this paper consisted of slow-rate roller-coaster maneuvers at altitudes of 20,000 and 30,000 feet. The maneuvers were about 12 to 15 seconds in duration, with the pilot smoothly pulling up from 1 g to approximately 1.8g, pushing over to 0.2g, then returning to 1 g. Speed ranges were from $M = 0.55$ to $M = 0.82$ at an altitude of 20,000 feet and from $M = 0.70$ to $M = 0.90$ at 30,000 feet.

The center of gravity was maintained at 26 ±1 percent of the mean aerodynamic chord by transferring fuel within the fuselage tanks. The average gross weight was approximately 290,000 pounds.

The Reynolds number, based on the wing mean aerodynamic chord, varied from 46×10^6 to 75×10^6.

RESULTS AND DISCUSSION

Flight Tests

Typical time histories of slow-rate roller-coaster maneuvers of the type analyzed are shown in figures 4 and 5 for Mach numbers of 0.70 and 0.86, respectively, at an altitude of 30,000 feet. For these maneuvers the airplane is approximately in balance at all times and the maneuvers are sufficiently slow that the wing structural frequencies are not excited (figs. 4 and 5). For the wing loads, in particular, the effects of pitching velocity and acceleration were examined and found to be negligible.

The wing loads measured during the maneuvers presented in figures 4 and 5 are shown in figures 6 and 7 as the variation of the loads with the normal acceleration measured at the airplane center of gravity. The aerodynamic shear, bending moment, and torque are presented for the six stations along the wing. For each of the wing stations indicated in figure 3 the measured load is the aerodynamic load outboard of a line perpendicular to the elastic axis at the particular wing station. The bending moment is measured about the same line perpendicular to the elastic axis, and the torque is measured around the elastic axis. Note that the slope of the elastic axis is discontinuous at a point between wing stations 444 and 600 (fig. 3); therefore, the torque and bending-moment measurements are not directly comparable inboard and outboard of this discontinuity. In order to illustrate as simply as possible the effects of Mach number and lift on the wing loads only the loads at the inboard station (wing station 222) are shown subsequently, since the inboard station loads reflect the changes which occur on the outer panel.

Figures 8 and 9 present the variation with airplane normal-load factor of the aerodynamic shear, bending moment, and torque measured at the typical wing station (wing station 222) for the speed ranges of the tests at altitudes of 20,000 and 30,000 feet. The variation of the shear and bending moment with normal acceleration at both altitudes is essentially linear. Some nonlinearity is apparent in the torque curves for an altitude of 20,000 feet. At an altitude of 30,000 feet the nonlinearity is even more pronounced in the torque data. At the higher lifts there is a tendency for the curves to flatten out to a slope near neutral. With increasing Mach number this change in slope becomes more pronounced and occurs at lower values of lift. At the highest test Mach number, the slope is approximately zero over the entire lift range investigated. The change in the variation of torque with normal-load factor to a neutral or slightly negative slope indicates a rearward movement of the center of pressure with increasing lift or Mach number. This trend of the center-of-pressure movement is typical of transonic flow characteristics.

It should be noted that the torque data obtained at an altitude of 30,000 feet not only evidence nonlinearities but there are large loops or scatter apparent in the data, particularly at the higher Mach numbers. By referring to the time histories of typical maneuvers in figures 4 and 5, it is apparent that losses in Mach number and dynamic pressure occur in all the maneuvers, primarily in the initial pull-up phase of the maneuvers. It is believed, however, that these loops or scatter at the higher Mach numbers ($M = 0.86$ and $M = 0.90$) are caused by a combination of the Mach number changes and the inherently unstable flow conditions that exist when the local flow is changing from subsonic to supersonic as evidenced by the relatively rapid rearward movement of the aerodynamic center that occurs in this Mach number range.

To illustrate more fully the Mach number and altitude effects on the measured wing loads, these loads are summarized in figures 10 and 11. Figure 10 presents the variation with both Mach number and dynamic pressure of the basic air load, that is, the wing shear, bending moment, and torque intercepts at zero airplane acceleration. Figure 11 presents the variation with Mach number and dynamic pressure of the aerodynamic center and the spanwise center of pressure of the additional air load. These data were obtained by taking slopes of the curves in the lower lift region where the data are essentially linear. Figure 10 shows no significant changes in the basic air-load curves of shear or bending moment with either Mach number or dynamic pressure, but the basic air-load torque curves indicate combined effects of both Mach number and dynamic pressure. The center-of-pressure variations shown in figure 11 indicate an inboard shift of the center of pressure of the additional load and a forward movement of the aerodynamic center as Mach number or dynamic pressure is increased. For speeds up to $M = 0.86$, the trends are typical for a subsonic sweptback flexible wing. It may be noted that for this speed range the locus of the centers of pressure fall near the wing quarter-chord line. The points at the two highest Mach numbers are somewhat more

interesting in that a rearward transonic aerodynamic-center shift occurs. It should be reemphasized that the aerodynamic-center and additional-load center-of-pressure data are for the lower lift regions only. It should be recalled that the torque curves of figure 9 show that the rearward movement of the aerodynamic center actually started at a Mach number of approximately 0.82 and a normal acceleration of 1.4g which corresponds to an airplane normal-force coefficient of 0.35. As Mach number is increased from 0.82 to 0.90, the lift coefficient at which the aerodynamic center moves rearward decreases until at $M = 0.90$ the aerodynamic center is in the rearmost position for the total lift region covered.

Presented in figures 12 and 13 are the span-load distributions and the deflections along the wing for Mach numbers of 0.70, 0.82, 0.86, and 0.90 at an altitude of 30,000 feet. These data are typical of the data at the other Mach numbers and at the lower altitude. Both the span-load distribution and the wing-deflection curves are presented per unit normal-load factor, and are for the lower lift range. Since the loads are referenced to the wing axis system, streamwise or spanwise bending moments or torque are not represented. Because the nacelle air load is introduced into the wing structure at the nacelle locations, the spanwise distribution of torque has discontinuities (fig. 12) at these locations. It should be noted that the loads reference axis is also rotated near the inboard nacelle, producing an additional discontinuity in torque and bending moment at this wing station. The previously discussed rearward shift in the aerodynamic center at the higher Mach numbers is reflected in the changed shape of the torque distribution between the lowest and highest test Mach numbers. In addition, the nacelle effects mentioned previously are also present in the shear and bending-moment curves, but to a much lesser extent. Therefore, the shear and bending-moment curves are faired smoothly.

The deflection curves presented in figure 13 show only the wing bending. A reduction of about 18 percent is apparent in the wing-tip bending deflection per unit normal-load factor as Mach number is increased from 0.70 to 0.90. This reduction in bending deflection is associated with the inboard and forward movement of the center of pressure as Mach number and dynamic pressure increase. The maximum predicted and measured twist per unit normal-load factor along the wing axis were each less than 1° over the speed range of these tests. However, the variation of the measured twist was irregular because of reading errors in the measurements, therefore, the variations of the measured twist are not presented.

Air-Load Calculations

Method and data used in the analysis.- In the experimental data presented previously both Mach number and flexibility effects were present. For a better understanding of these combined effects, calculations of the air loads were made for several maneuvers by using one of

the available methods, the method of reference 1. This method, which is, in essence, based on lifting-line theory makes use of experimental wind-tunnel data for determining the air loads on a flexible wing. Ten control points on each wing semispan, resulting in 10 simultaneous equations, were used to determine the wing span-load distribution. In addition, equations for total airplane lift and balance were included, which resulted in a system of 12 simultaneous equations to be solved for the various flight conditions. The calculated structural properties of the B-52 and the necessary aerodynamic characteristics determined from wind-tunnel tests were obtained from Boeing Airplane Company.

The basic quantities required for the calculations are shown in figure 14. Presented in figure 14(a) is the section lift-curve-slope variation along the span at $M = 0$ as derived from wind-tunnel tests. The Prandtl-Glauert Mach number correction for swept wings $\frac{1}{\sqrt{1 - M^2 \cos^2\Lambda}}$ was used to correct the section lift-curve slopes. Figure 14(b) presents the section net zero-lift angles which include the geometric built-in incidence and aerodynamic interference. The calculated spanwise deadweight distributions are shown in figures 14(c) to 14(e). The change in total airplane pitching moment for nacelles off and on and external tank off and on was obtained from wind-tunnel data supplied by the manufacturer. The air loads on the nacelles and external tank were derived from these wind-tunnel data and used in the calculations as pure couples with zero normal force. The calculated wing stiffness distributions are shown in figure 14(f).

In order to obtain some assessment of the reliability of the calculated stiffness distribution, the calculated stiffness distribution was compared with some available experimental data. The data consisted of measurements of the wing-tip deflections during the loading required for the strain-gage calibration. In figure 15 the deflections are plotted against the wing stations at which the loads were applied. The square symbols of this figure present experimental deflections for wing station 1325 as the deflection per pound of load applied at various wing stations. The circular symbols indicate the results obtained by using the estimated wing stiffness to calculate the deflections. The calculated deflections are appreciably higher than the measured deflections which indicates that the wing is somewhat stiffer than originally estimated. Since the estimated stiffness (fig. 14) was based on a wing-root stiffness which was reduced to account for sweepback in the wing center section, making the front spar relatively less effective, the deflections were recalculated neglecting the estimated reduction in stiffness at the wing root. The results of this calculation are shown by the diamond symbols. Again, it may be noted that the calculated deflections are considerably higher than the measured deflections. Next, the deflections were calculated by using an assumed 20-percent increase in the stiffness distribution and the results of this calculation are shown by the triangular symbols. This calculation resulted in good agreement between the measured

and the calculated deflections. This increase in bending stiffness was also checked by comparing the wing deflection measured in flight with the deflection calculated by using the measured load and the increased stiffness. The results of this comparison are shown in figure 16. The comparison indicates that the 20-percent increase in wing bending stiffness results in generally good agreement between the measured and the calculated deflections.

Calculations of the air loads were made for the originally estimated bending stiffness, the 20-percent increase of bending stiffness, and for a rigid wing. For convenience in the calculation employing a 20-percent increase in bending stiffness, a factor of 20 percent was applied to all values of the structural matrix, which has the effect of also increasing the torsional stiffness by 20 percent.

Results of air-loads calculations including effects of varying stiffness distribution.- Figure 17 illustrates the results of these calculations for Mach numbers of 0.56, 0.70, and 0.82 at an altitude of 20,000 feet and Mach numbers of 0.70, 0.82, 0.86, and 0.90 at 30,000 feet. The distributions of shear, bending moment, and torque with wing station are presented. It should be noted that these quantities are referenced to the wing axis system and do not represent spanwise distributions of bending moment and torque. The measured data are represented by the square symbols, whereas the results of the calculations using the estimated stiffness are shown by the circular symbols, and the results of increasing the wing stiffness are shown by the diamond symbols. The results of a rigid-wing calculation as well as the results of the flexible-wing calculations are shown in figure 17(g) for a Mach number of 0.90 at 30,000 feet. Generally, the comparisons of the measured and calculated flexible-wing air loads shown in figure 17 are reasonably good and the discrepancies are of an order to be expected when theory and flight-test data are compared. By using the original stiffness distribution, the calculated bending moments and shear are underestimated and the torque values are overestimated for the inboard wing stations. The calculated shear curve is in better agreement with the flight-test data than either the bending-moment or torque curves. It is believed that for design purposes the discrepancies in torque would be relatively insignificant for this high-aspect-ratio wing since the wing strength normally would be established from the bending loads rather than from the torque loads. The effect of the increased wing stiffness is to increase somewhat the outboard loading and, therefore, the bending moments. This result is generally true for a sweptback wing with high aspect ratio where bending deflections are larger and more important than twist around the wing axis. Although increasing the stiffness has produced a somewhat closer correlation between the measured and predicted bending moment and shear, the resulting change was relatively minor in relation to the discrepancies which originally existed between the measured and calculated

bending moment. The effect of the increased stiffness was negligible on the calculated torque curves. The small inconsistencies between the two calculations of torque at the various speeds are the result of rounding off the data in the solutions.

The result of the rigid-wing calculation shown in figure 17(g) was to increase the root bending moment by about 24.5 percent and the root shear by about 7.5 percent over the results of the calculation using the estimated wing stiffness.

The differences between the measured and calculated bending moments are predominant in the area inboard of the nacelle locations for the bending-moment curves and at the nacelle stations in the torque curves. Since the agreement between the measured and calculated flexible-wing air loads was much better outboard of the two nacelles for both the original calculations and the calculations using the increased wing stiffness, the effect of varying the nacelle air loads in the calculations was investigated. As discussed previously, the nacelle air loads were determined from wind-tunnel tests of the complete airplane model in which the change in airplane normal force and pitching moment were measured, nacelles off and nacelles on. Since the change in airplane normal force was so small in relation to the normal force of the total airplane, only the change in airplane pitching moment could be measured. Therefore, only a nacelle pitching moment was used in the preceding calculations. It was obvious, however, that the nacelles would also carry a normal load. To evaluate the effect of using a normal force as well as a pitching moment in the calculation, the pure couple at each nacelle was replaced by a normal force at 25 percent of the nacelle length, giving the same nacelle pitching moment about the loads reference axis at the nacelle station. This resulted in a normal force of about 2,800 pounds per unit normal-load factor at each nacelle, which corresponded to a nacelle lift-curve slope of about 0.03 per degree at $M = 0.86$. The wing loads were then recalculated using this nacelle load. The results of this calculation showed an increase in the root bending moment so that it agreed more closely with the measured bending moment, whereas the root shear was increased only slightly and the change in torque was negligible. Although the results of this calculation are not shown, the changed nacelle air load increased the calculated bending moment at wing station 173 (shown in fig. 17(f)) from 50.2×10^6 inch-pounds to 51.2×10^6 inch-pounds. The shear increased from 120,400 pounds to 121,800 pounds and there was no appreciable change in torque. This calculation and the earlier calculations indicate that the effect of the nacelle loads may be rather large in both bending moment and torque, and that for calculations of this type it may be important to have wind-tunnel data that adequately define the nacelle loads.

CONCLUDING REMARKS

The results of this investigation of the effects of flexibility on the wing loads of the Boeing B-52 airplane have, in general, agreed with the trends that might be expected for a swept wing with high aspect ratio. The following results are considered of general interest:

1. The effect of wing bending rather than twist about the wing axis appears to be predominant in changing the air-load distribution due to flexibility. Because the bending effect was predominant, the center of pressure moved inboard and forward with increasing dynamic pressure.

2. The rearward transonic aerodynamic-center movement starts near a Mach number of 0.82 for a lift coefficient of 0.35 and with increasing Mach number occurs at progressively lower lifts until at the highest test Mach number of 0.90, the aerodynamic center remains in the rearmost position over the total lift region investigated.

3. The measured loads were compared with the loads calculated by the method of NACA TN 3030 which makes use of experimental wind-tunnel data and calculated wing-structural properties. The comparisons of the measured and calculated loads indicated that this method of predicting the loads appears reasonable for airplane configurations of this general type and speed range.

4. To illustrate the effects on the air loads of varying the structural properties, calculations were made in which the wing stiffness was varied. A 20-percent increase in wing stiffness resulted in generally small changes in the calculated shear, bending moment, and torque curves for the altitude and Mach number range of these tests. For a Mach number of 0.9 at an altitude of 30,000 feet a rigid-wing calculation showed an increase in wing-root bending moment per unit normal-load factor of about 24.5 percent with a corresponding increase in root shear of about 7.5 percent.

5. Results of calculations in which the nacelle air loads were varied indicated that the nacelle air loads can have a strong influence on the

total wing loads and that an accurate estimation of the nacelle air loads may be important in predicting the wing loads.

High-Speed Flight Station,
National Advisory Committee for Aeronautics,
Edwards, Calif., March 13, 1957.

REFERENCE

1. Gray, W. L., and Schenk, K. M.: A Method for Calculating the Subsonic Steady-State Loading on an Airplane With a Wing of Arbitrary Plan Form and Stiffness. NACA TN 3030, 1953.

TABLE I - PHYSICAL CHARACTERISTICS

Airplane (this investigation):	
Weight, lb	Approximately 290,000
Center of gravity, percent mean aerodynamic chord	26 ±1
Wing:	
Area, sq ft	4,000
Span, in.	2,220
Airfoil section:	
Root	BAC 233
Tip	BAC 236
Aspect ratio	8.55
Taper ratio	0.398
Root chord, in.	371
Tip chord, in.	148
Mean aerodynamic chord, in.	275.5
Sweepback of quarter chord, deg	35
Incidence angle, deg	6.0
Aileron area, (including tabs), sq ft	77
Aileron tab area, sq ft	18
Wing panel (outboard of streamwise line through the intersection of wing station 222 and elastic axis):	
Area, sq ft	1,690
Span, in.	985.3
Root chord, in.	346
Tip chord, in.	148
Mean aerodynamic chord, in.	260.2
Span distance from airplane center line to mean aerodynamic chord, in.	551.5
Horizontal stabilizer:	
Total area, sq ft	900
Span, in.	624
Root chord, in.	332.3
Tip chord, in.	83.0
Mean aerodynamic chord, in.	232.6
Taper ratio	0.250
Aspect ratio	3.0
Sweepback of quarter chord, deg	35
Elevator area, sq ft	79
Elevator tab area, sq ft	6.8
Stabilizer angle, deg	+9, -4
Elevator angle, deg	±20
Elevator tab angle, deg	±20
Vertical tail:	
Total area, sq ft	460
Span, in.	366
Root chord, in.	302
Tip chord, in.	60
Mean aerodynamic chord, in.	208.0
Taper ratio	0.198
Aspect ratio	2.02
Sweepback of quarter chord, deg	35
Rudder area, sq ft	44.5
Rudder tab area, sq ft	3.4
Rudder deflection, deg	±20
Rudder tab deflection, deg	±20

CONFIDENTIAL

Figure 1.- Photograph of the Boeing B-52 airplane. E-2367

CONFIDENTIAL

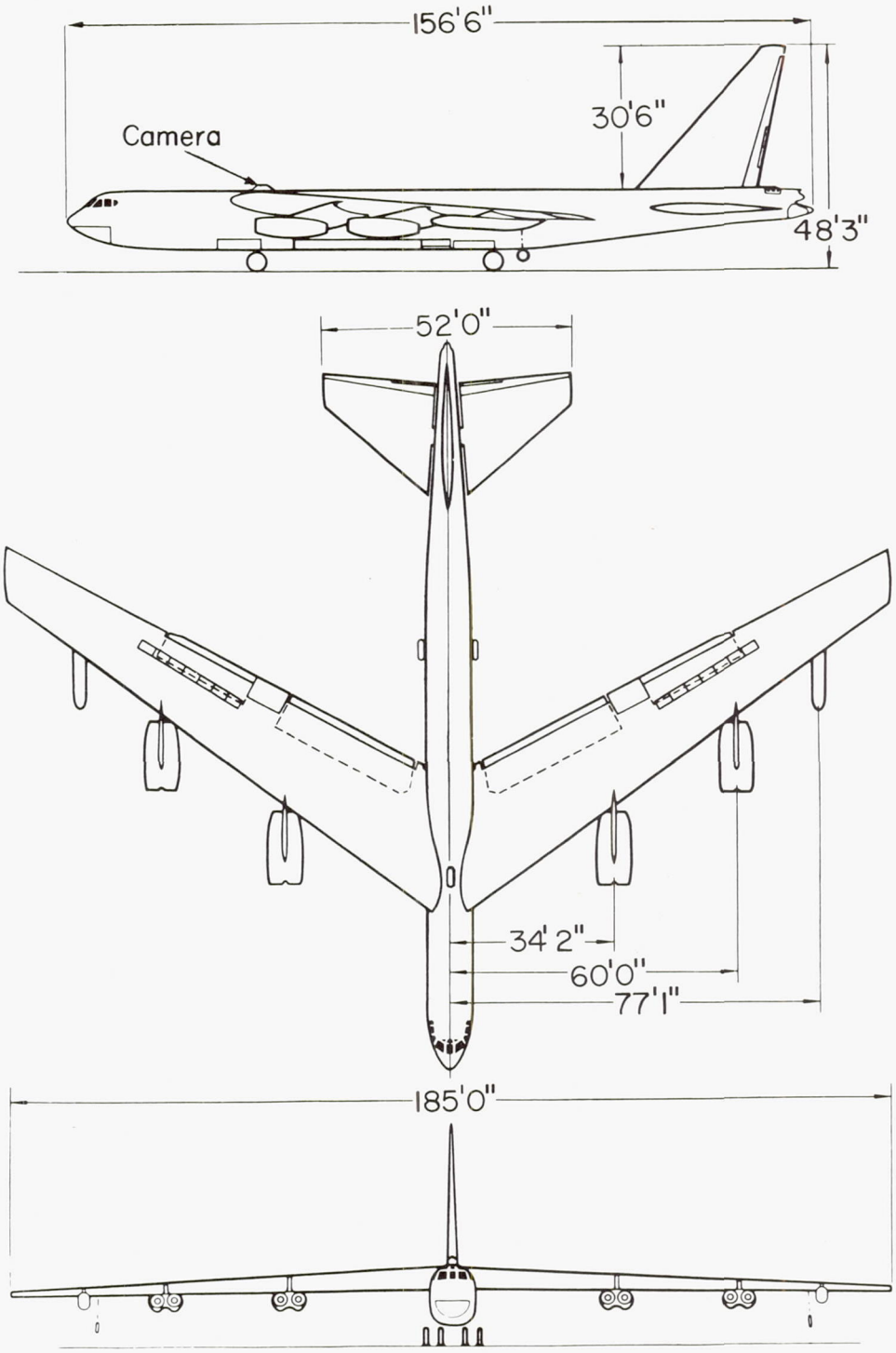

Figure 2.- Three-view drawing of the test airplane.

CONFIDENTIAL

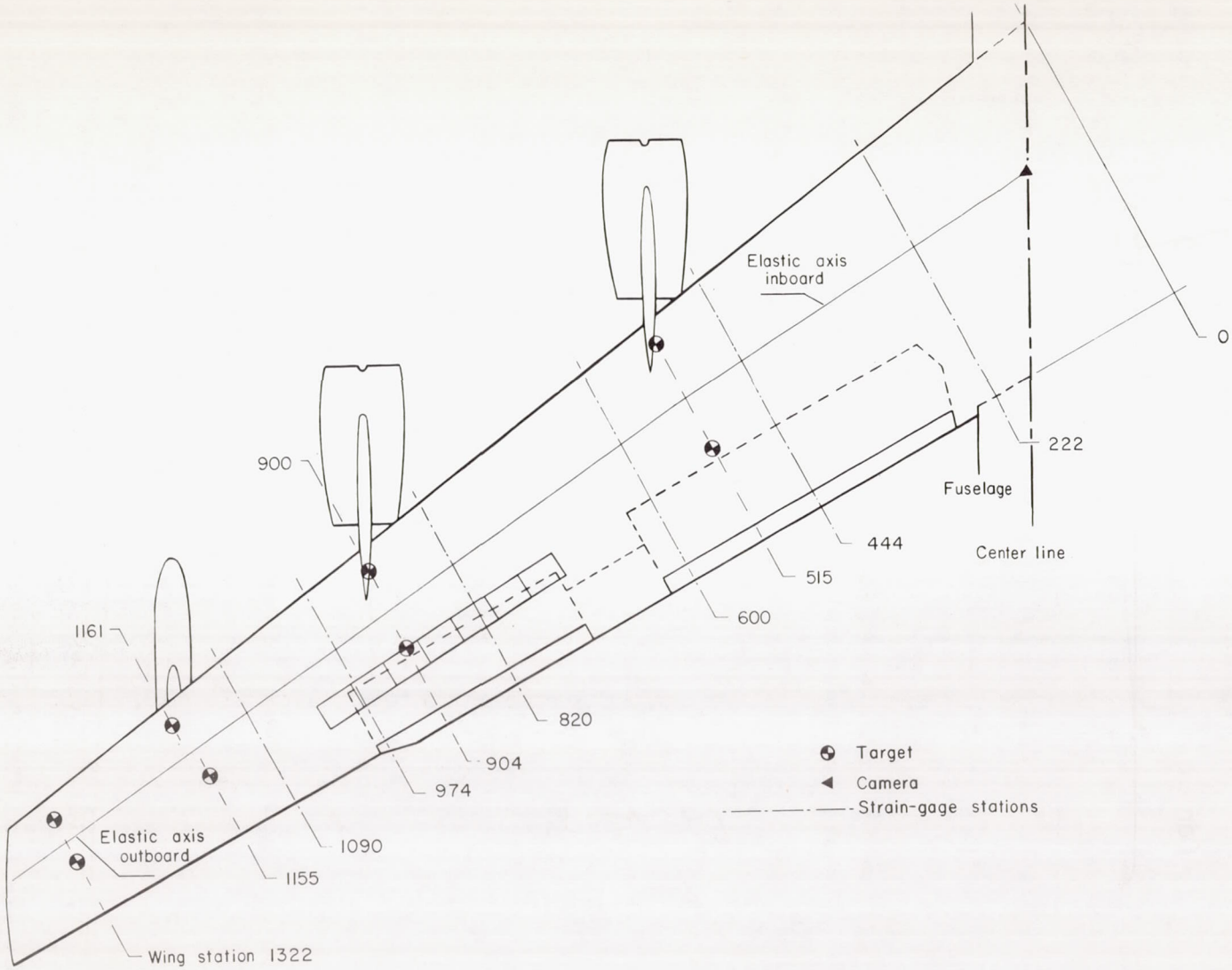

Figure 3.- Sketch of wing showing location of strain-gage stations, camera, and targets.

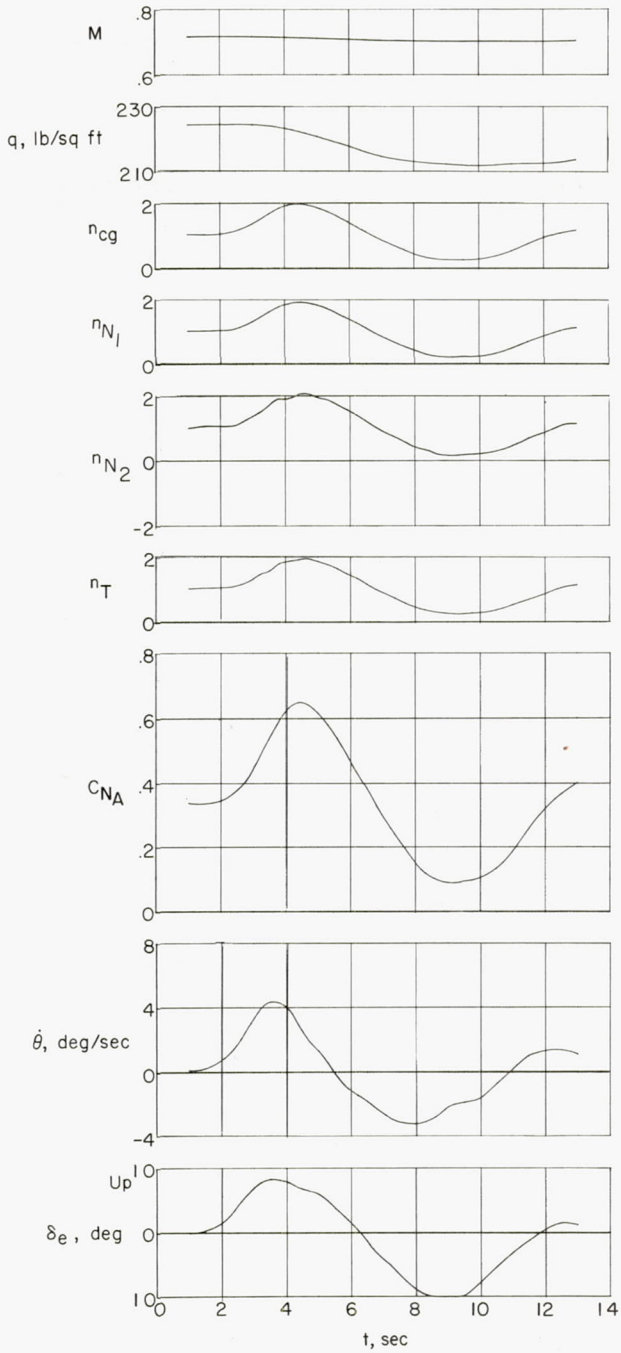

(a) Airplane response.

Figure 4.- Time history of a typical roller-coaster maneuver. $M \approx 0.70$; h_p = 30,000 feet; W = 291,000 pounds.

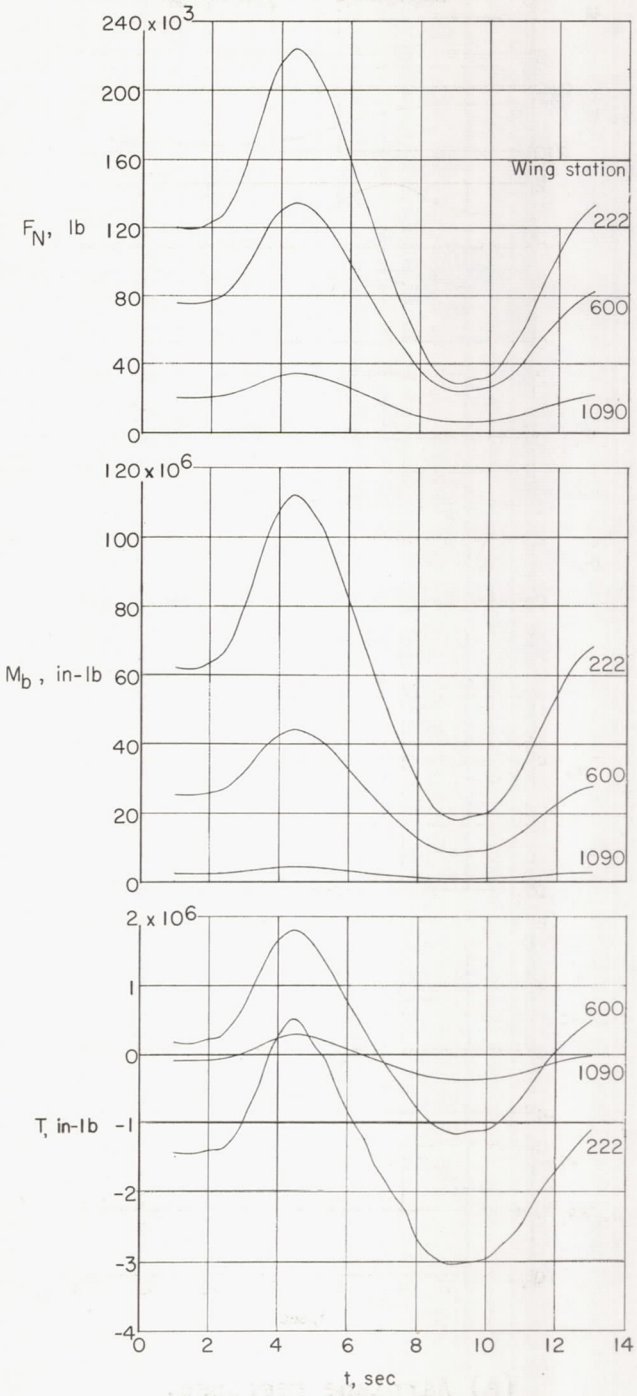

(b) Loads.

Figure 4.- Concluded.

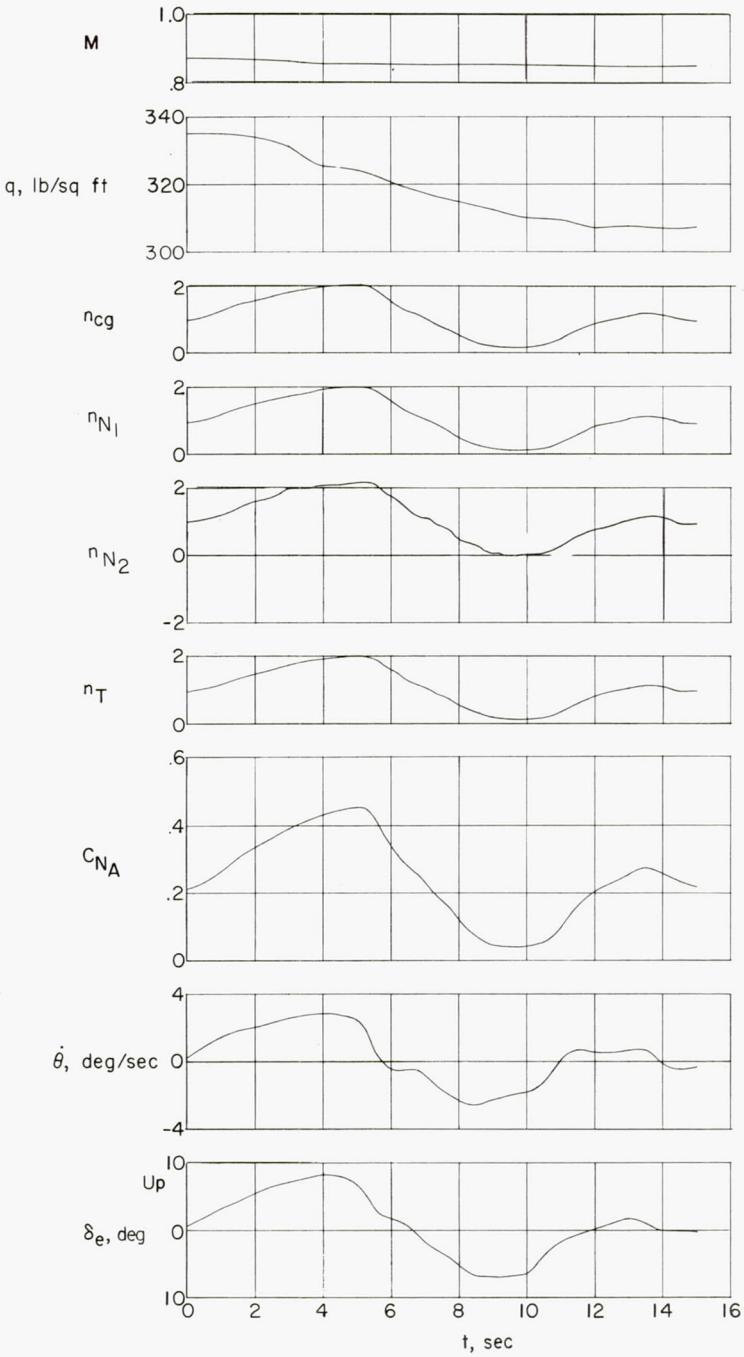

(a) Airplane response.

Figure 5.- Time history of a typical roller-coaster maneuver. $M \approx 0.86$; h_p = 30,000 feet; W = 286,600 pounds.

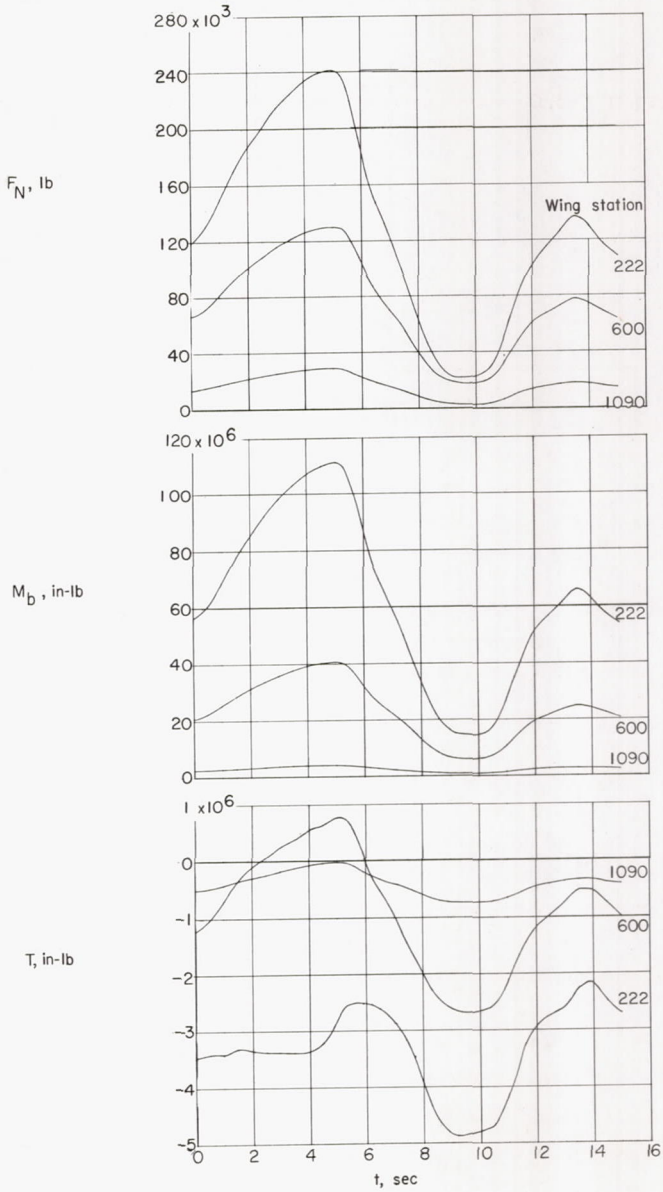

(b) Loads.

Figure 5.- Concluded.

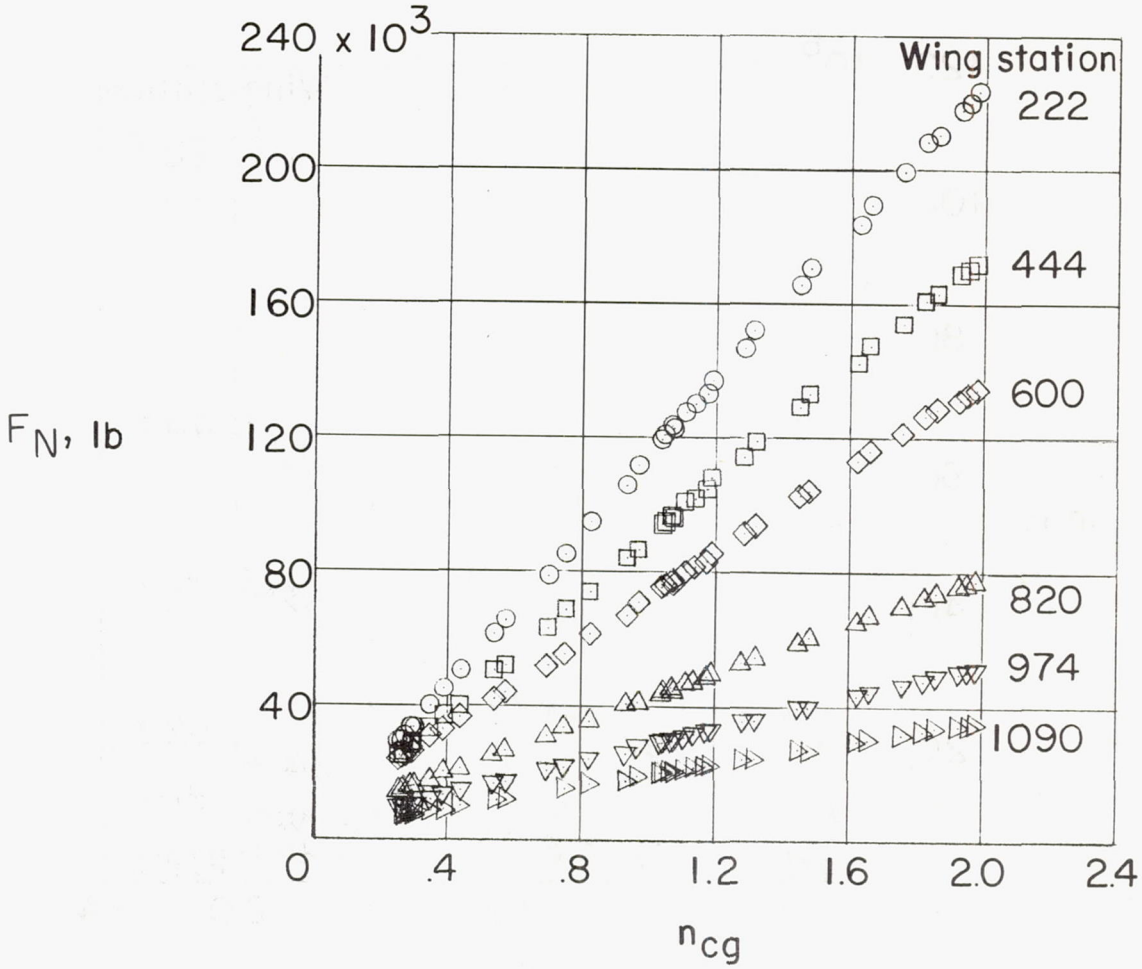

(a) Shear.

Figure 6.- Variation of aerodynamic wing loads at various wing stations with airplane normal-load factor. $M \approx 0.70$; $h_p = 30{,}000$ feet; $W = 291{,}000$ pounds.

DECLASSIFIED

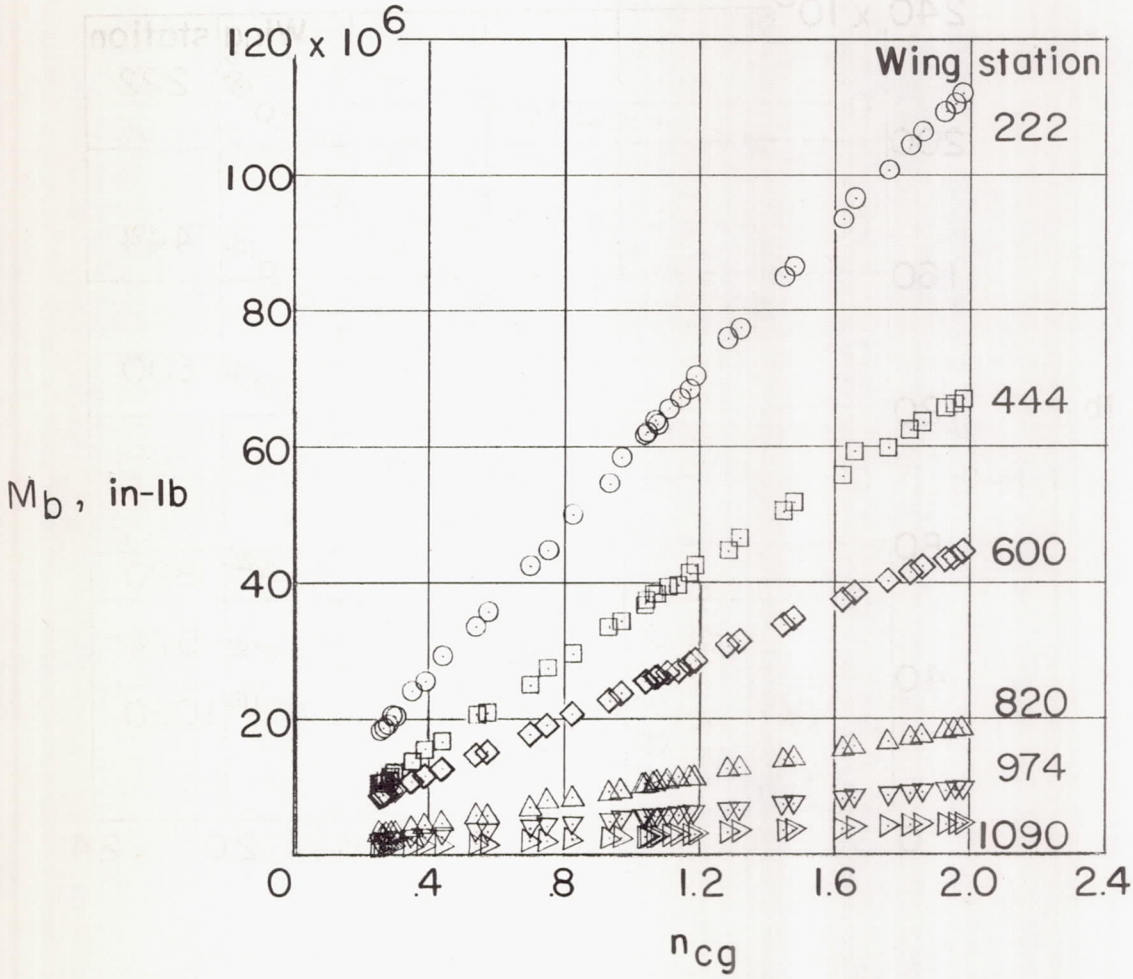

(b) Bending moment.

Figure 6.- Continued.

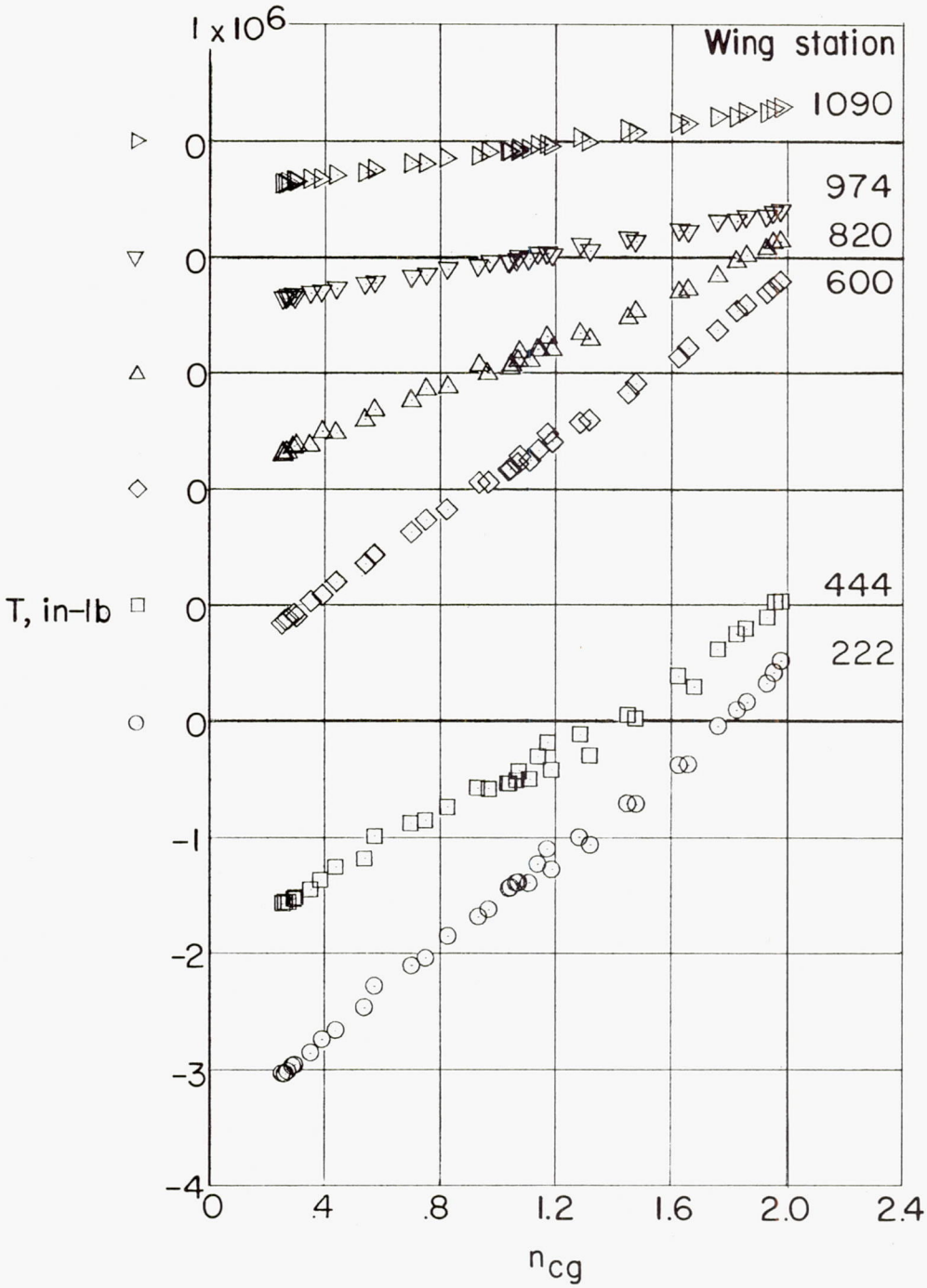

(c) Torque.

Figure 6.- Concluded.

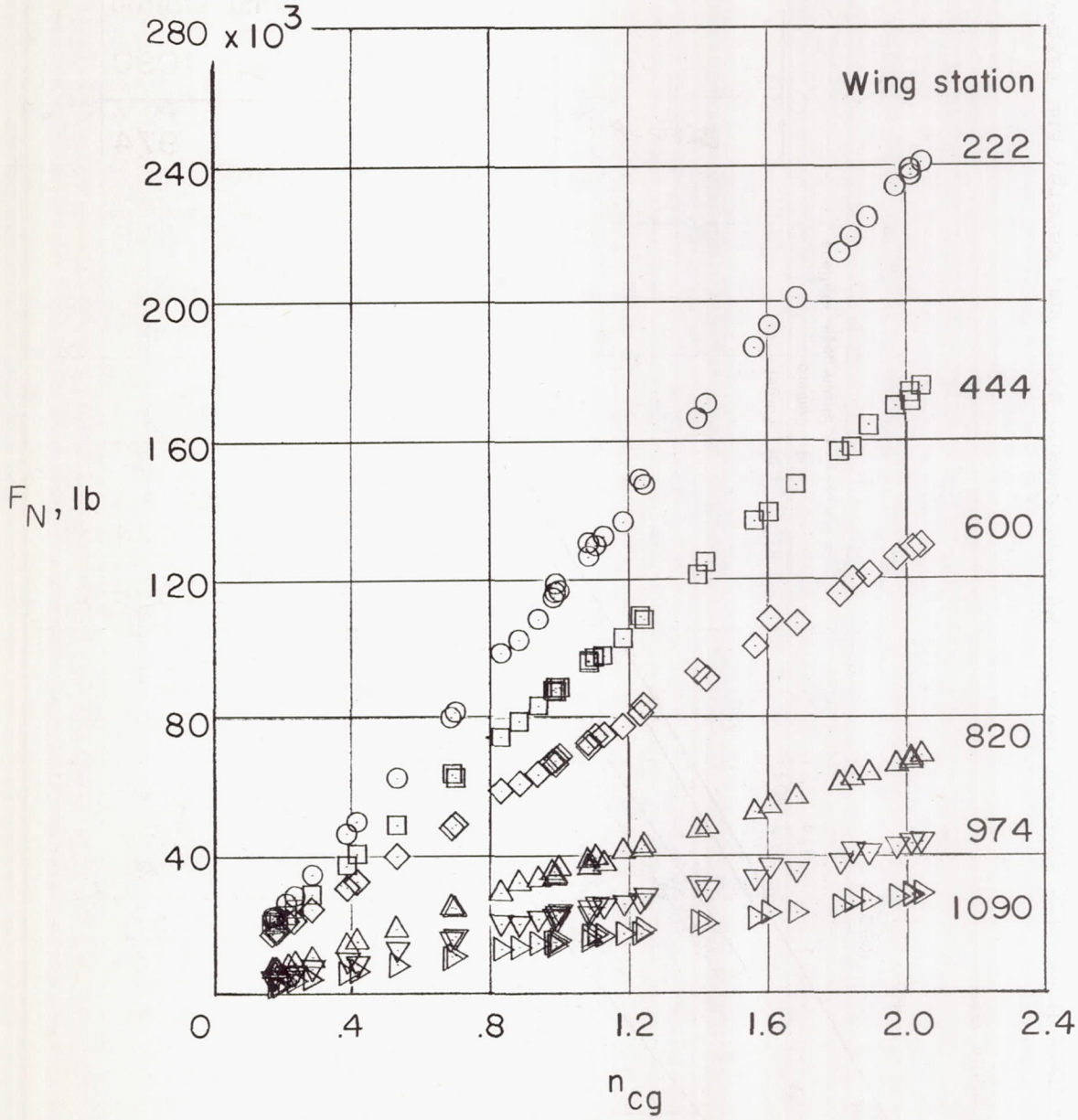

(a) Shear.

Figure 7.- Variation with airplane normal-load factor of aerodynamic wing loads at various wing stations. $M \approx 0.86$; $h_p = 30{,}000$ feet; $W = 286{,}600$ pounds.

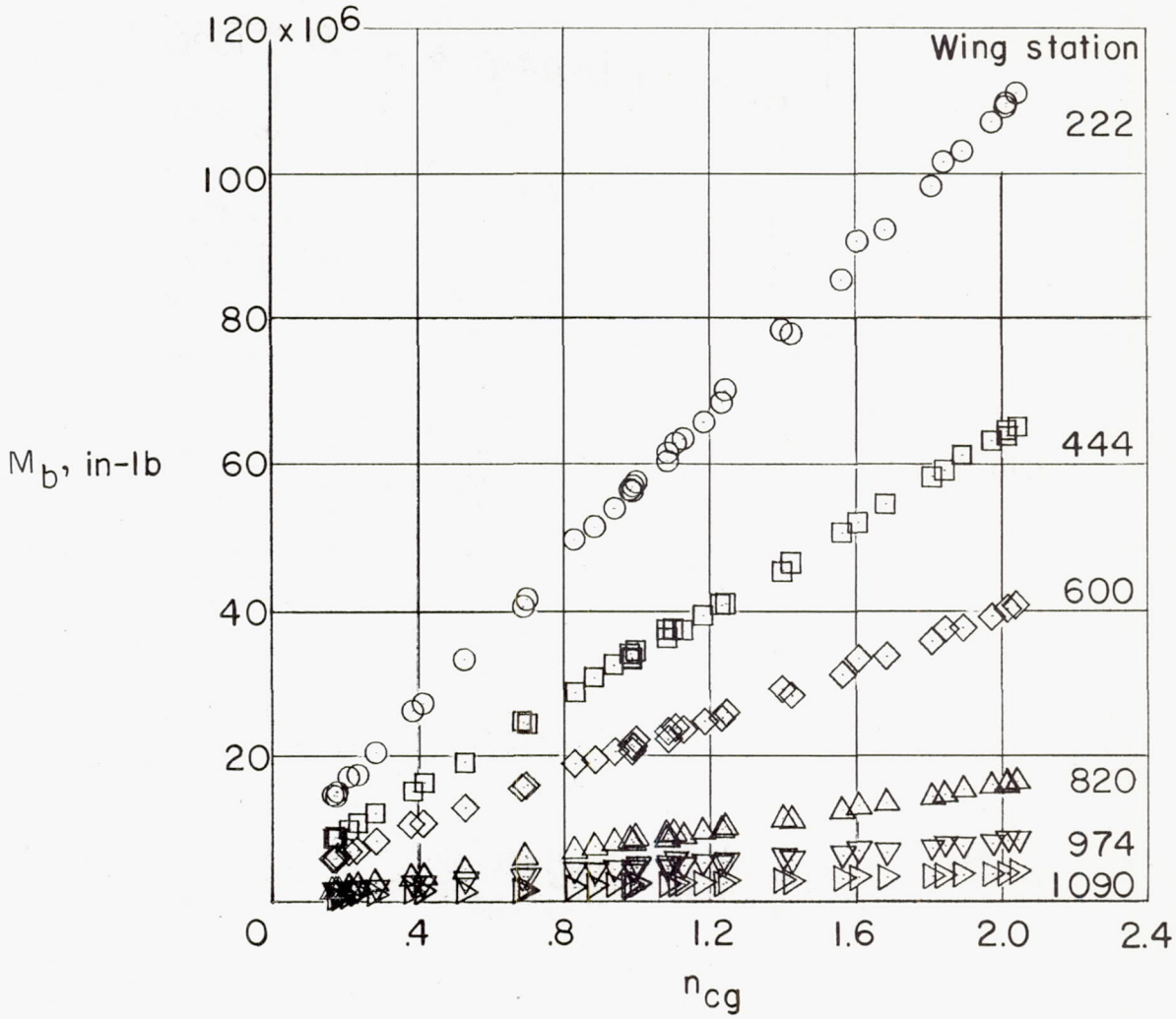

(b) Bending moment.

Figure 7.- Continued.

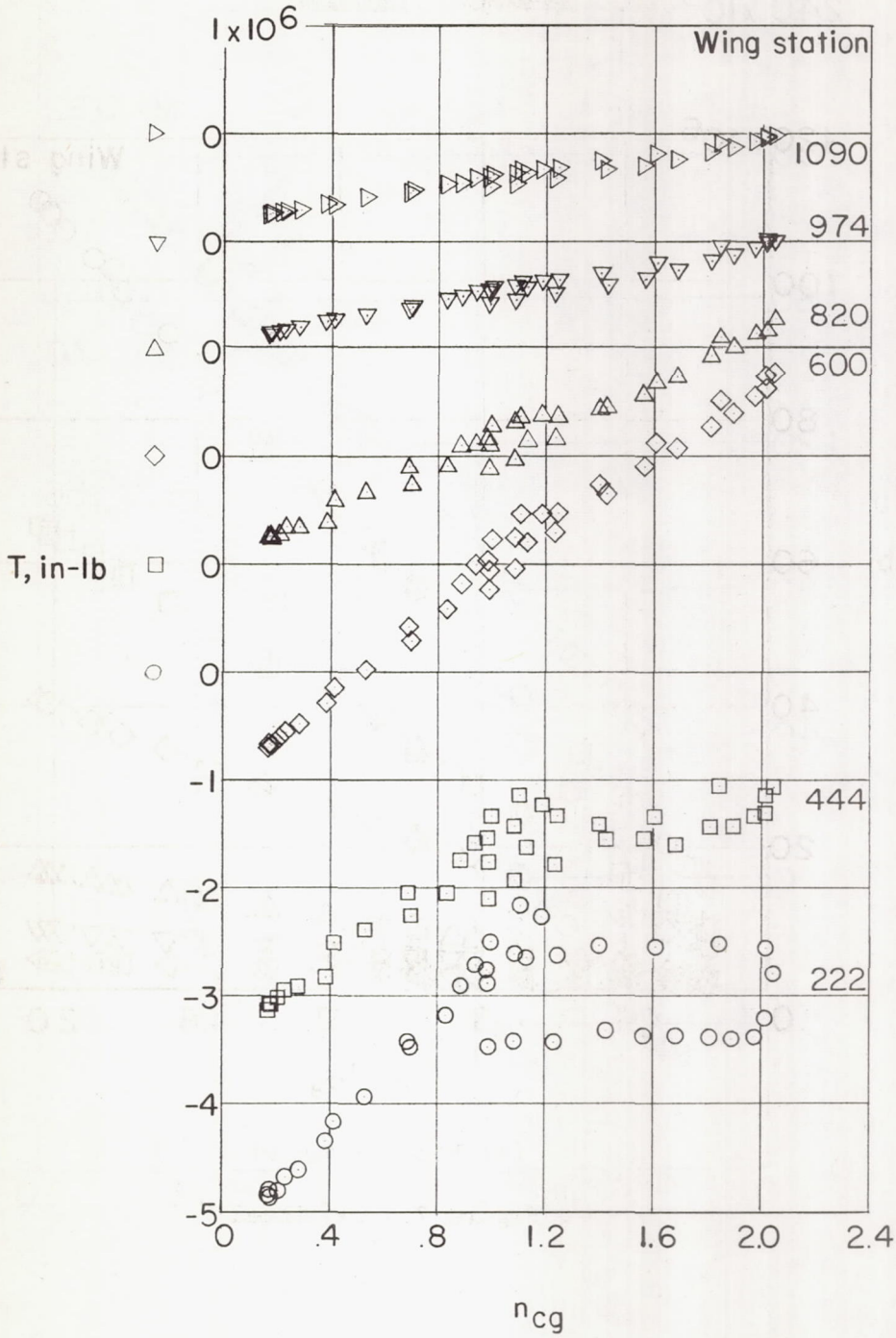

(c) Torque.

Figure 7.- Concluded.

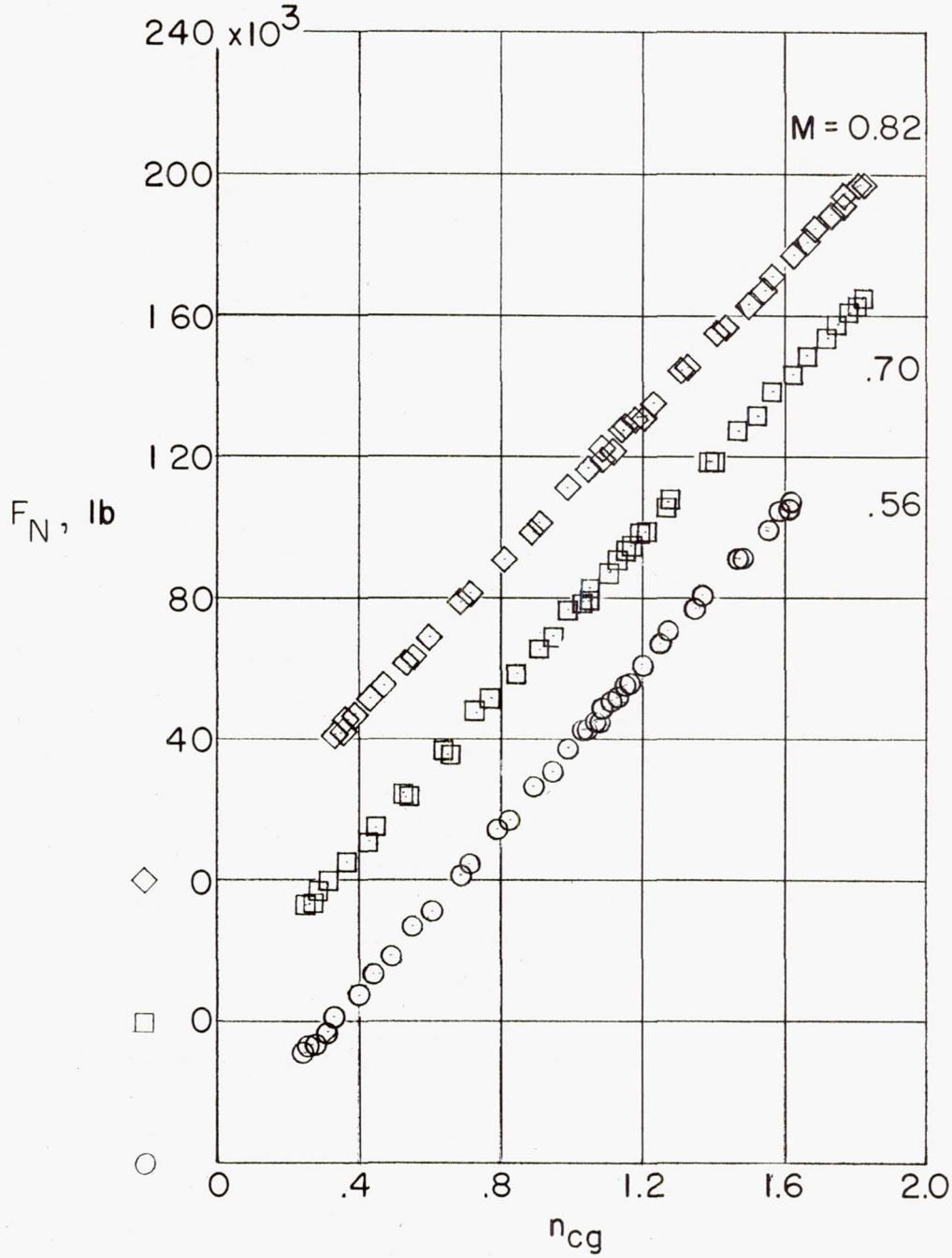

(a) Shear.

Figure 8.- Variation of wing root-station (wing station 222) loads with normal-load factor at various Mach numbers. h_p = 20,000 feet.

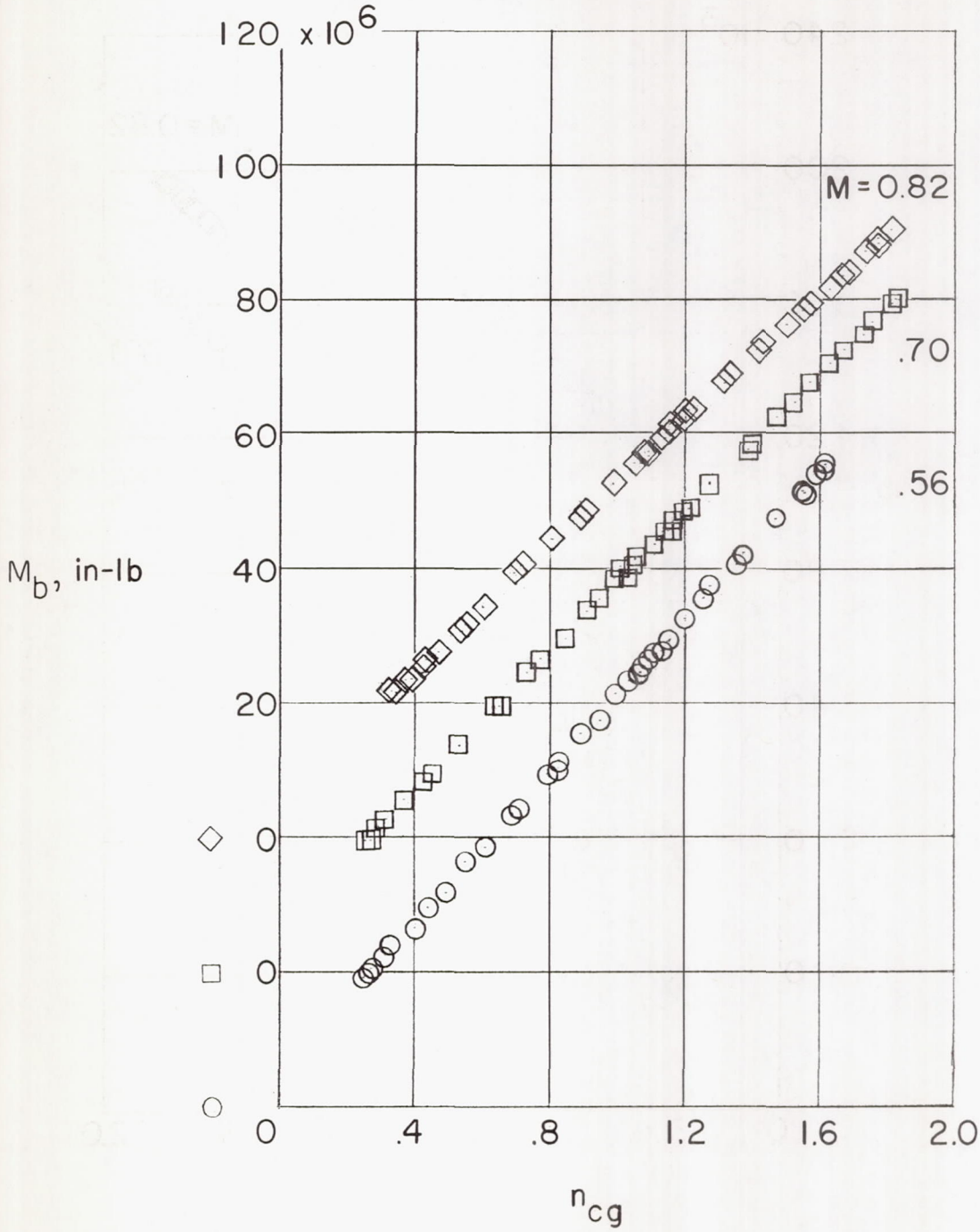

(b) Bending moment.

Figure 8.- Continued.

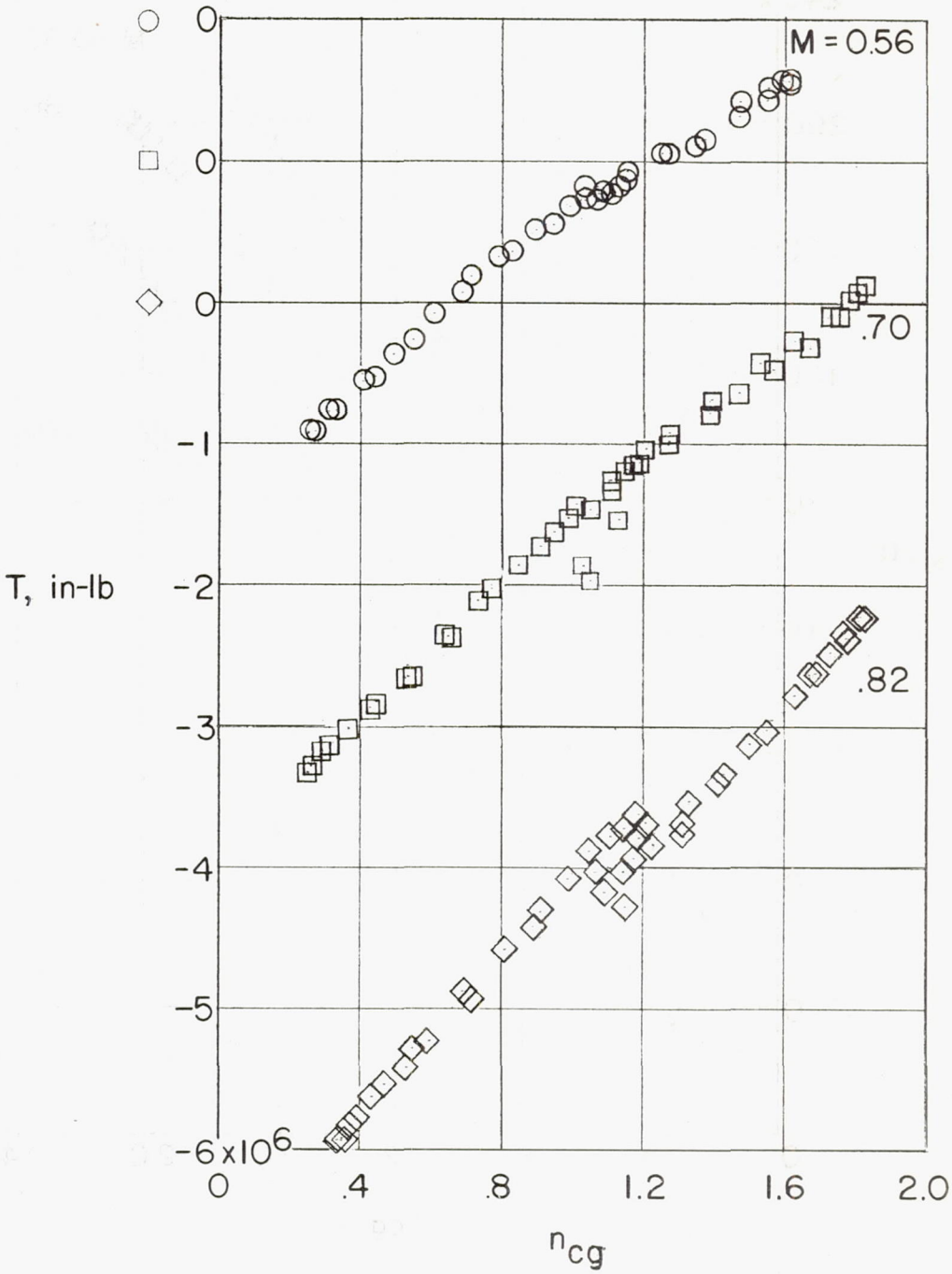

(c) Torque.

Figure 8.- Concluded.

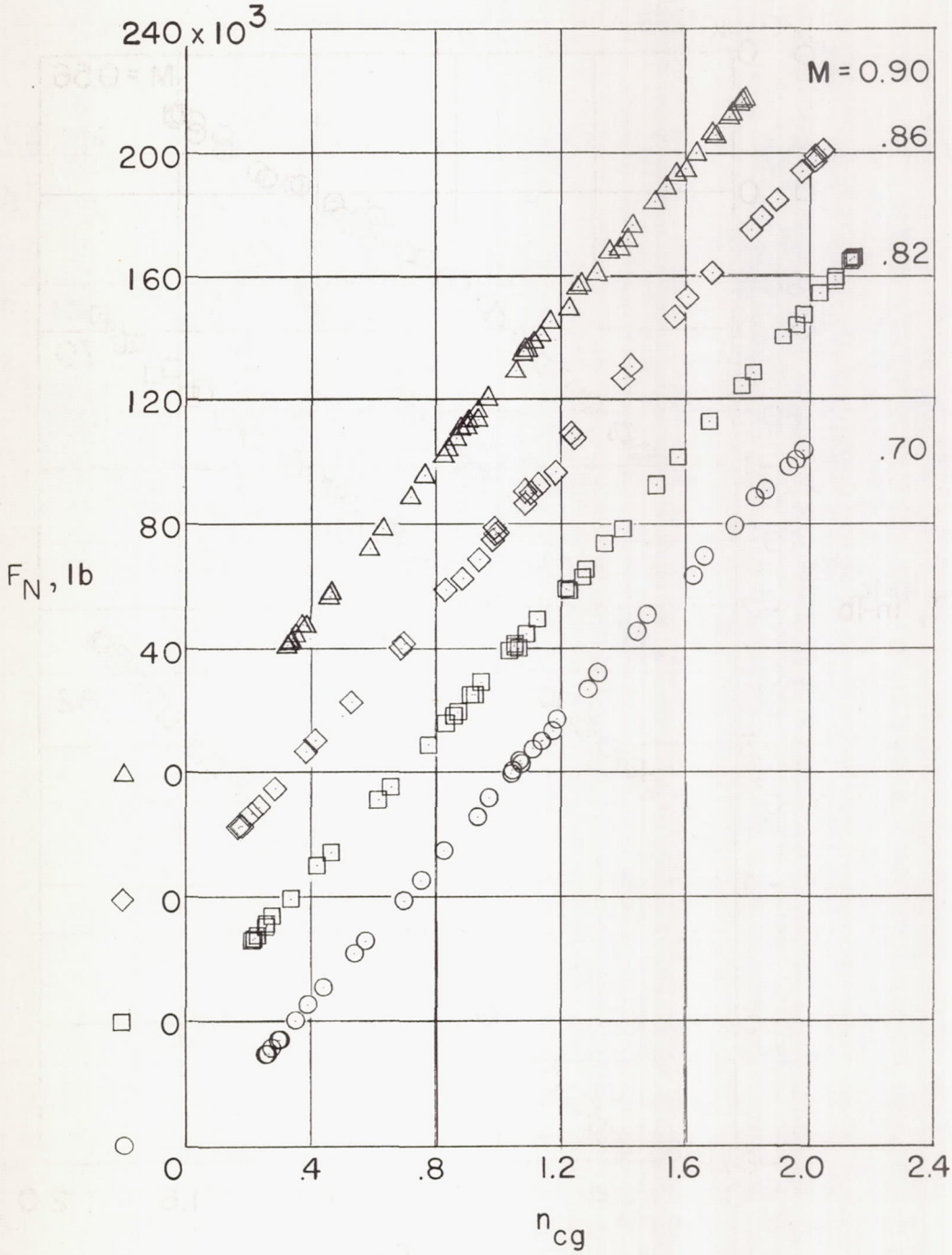

(a) Shear.

Figure 9.- Variation of wing root-station (wing section 222) loads with normal-load factor at various Mach numbers. h_p = 30,000 feet.

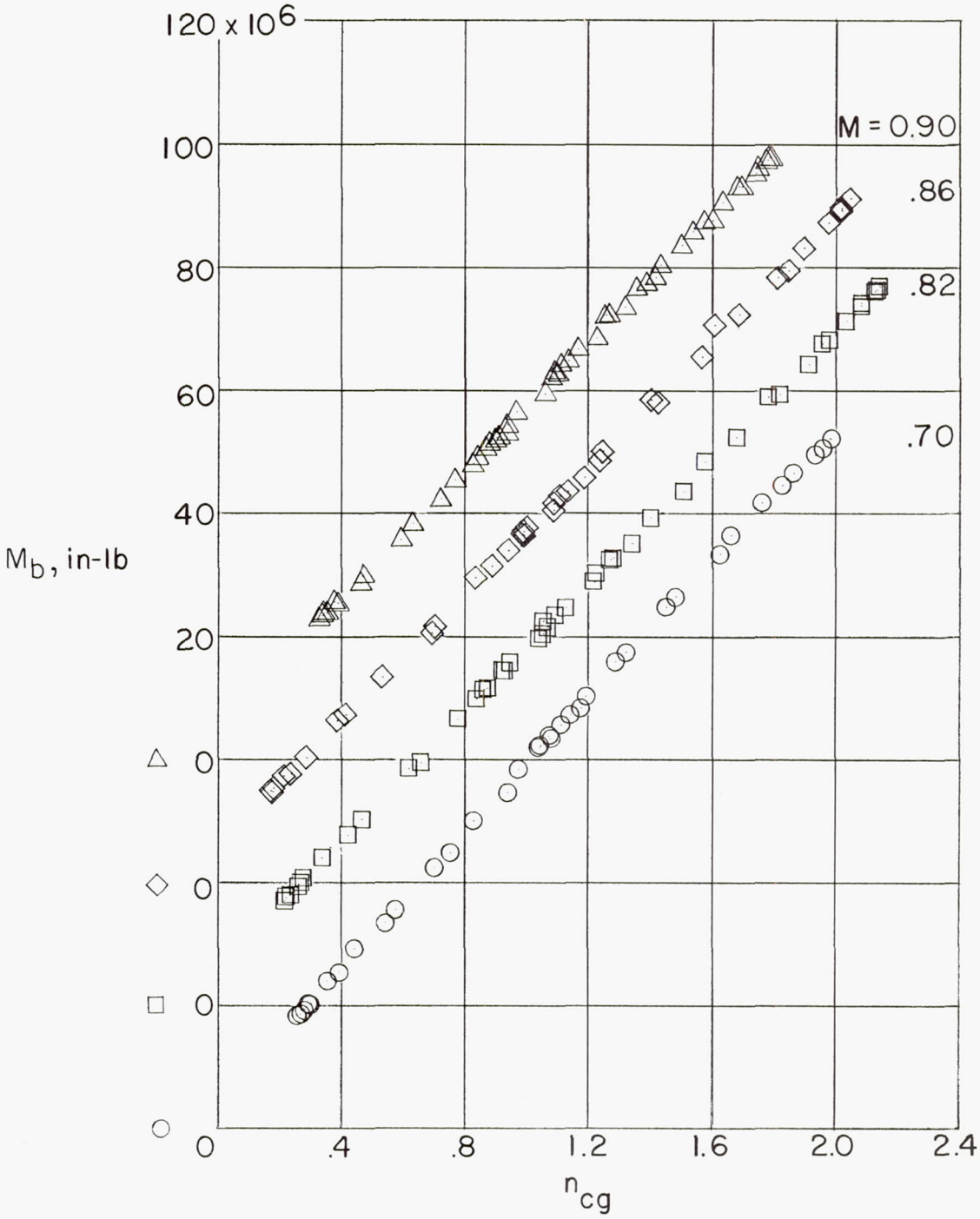

(b) Bending moment.

Figure 9.- Continued.

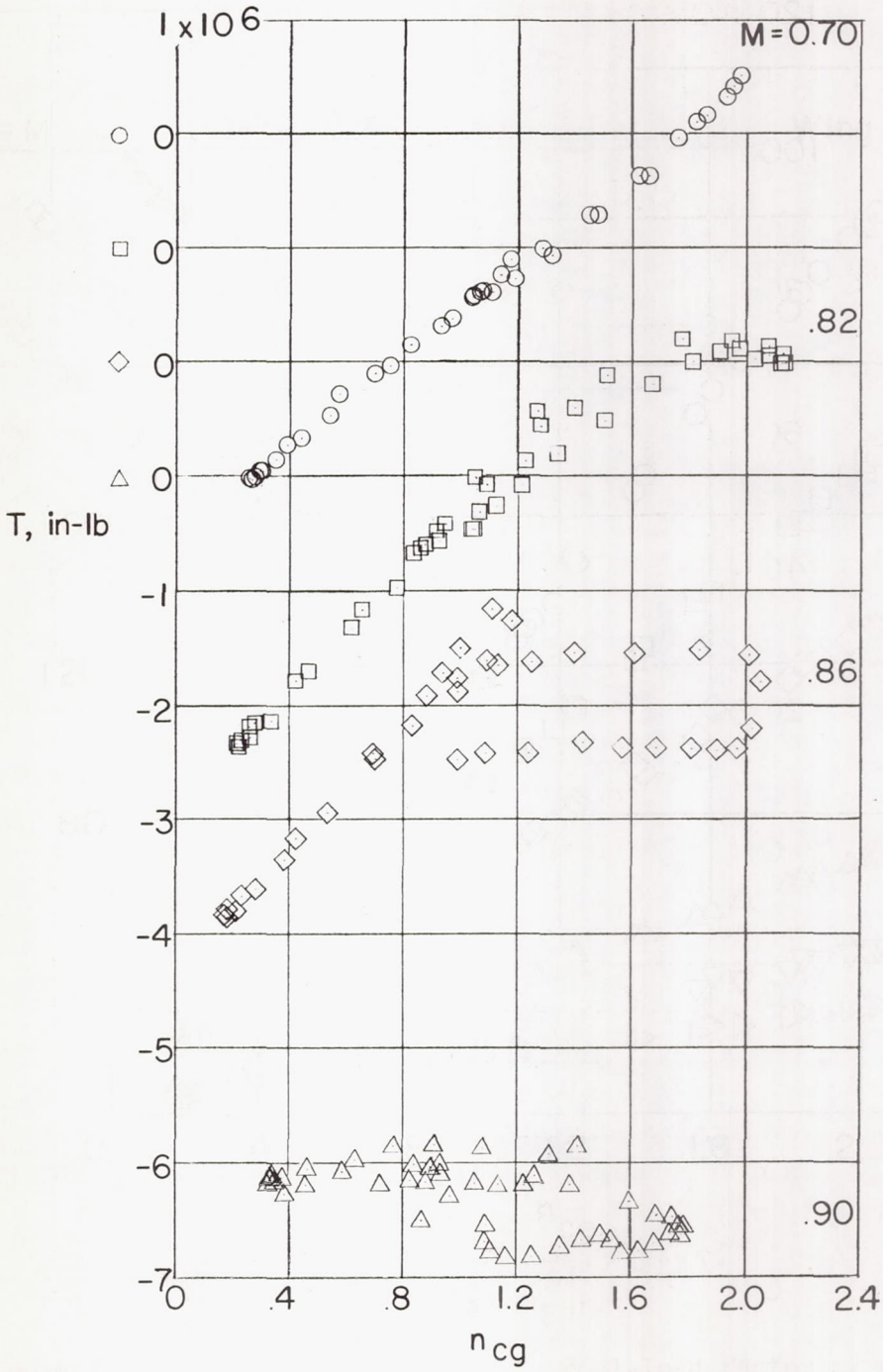

(c) Torque.

Figure 9.- Concluded.

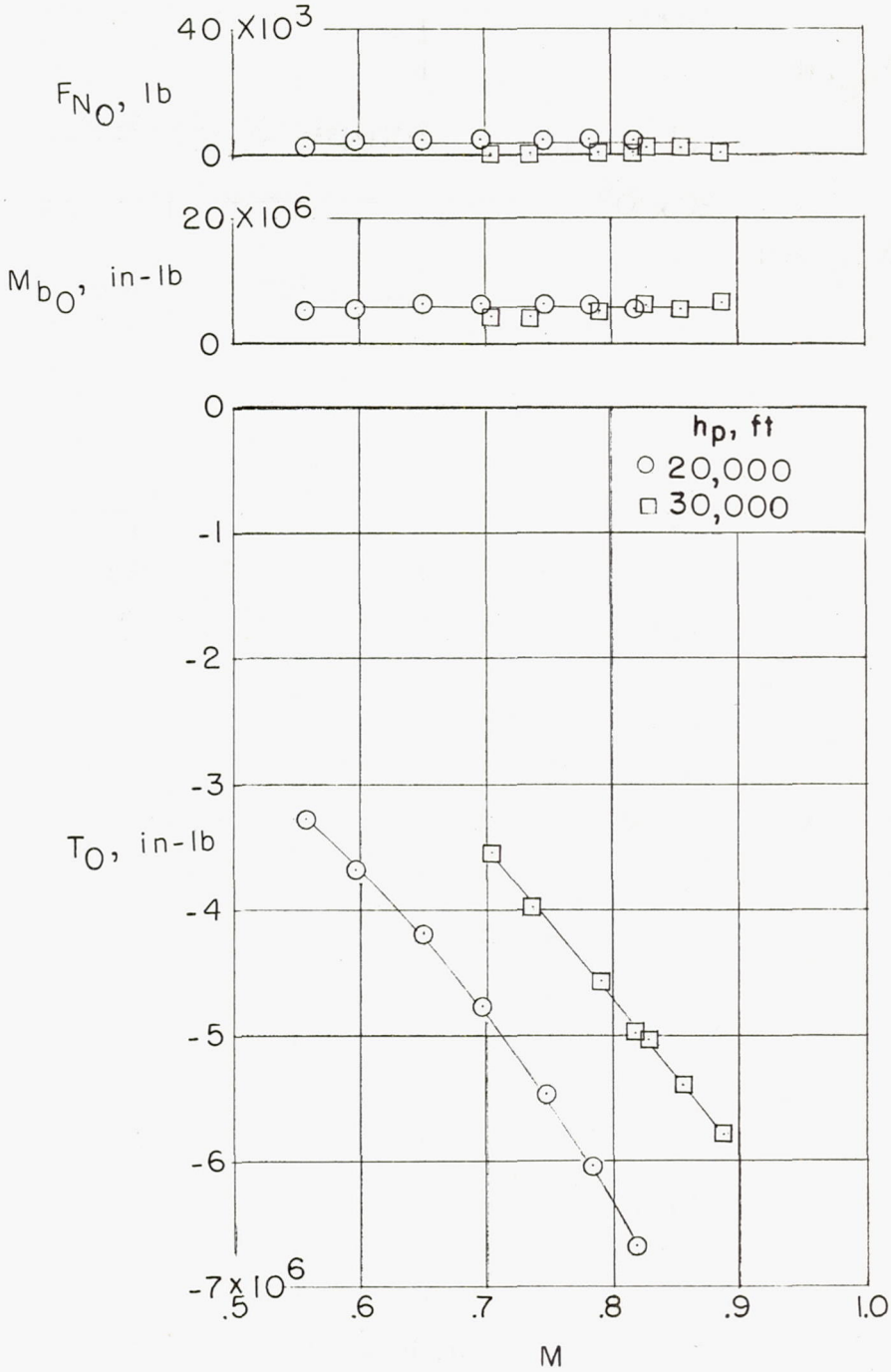

(a) Mach number.

Figure 10.- Variation with Mach number and dynamic pressure of wing root station (wing station 222) loads at zero airplane normal-load factor.

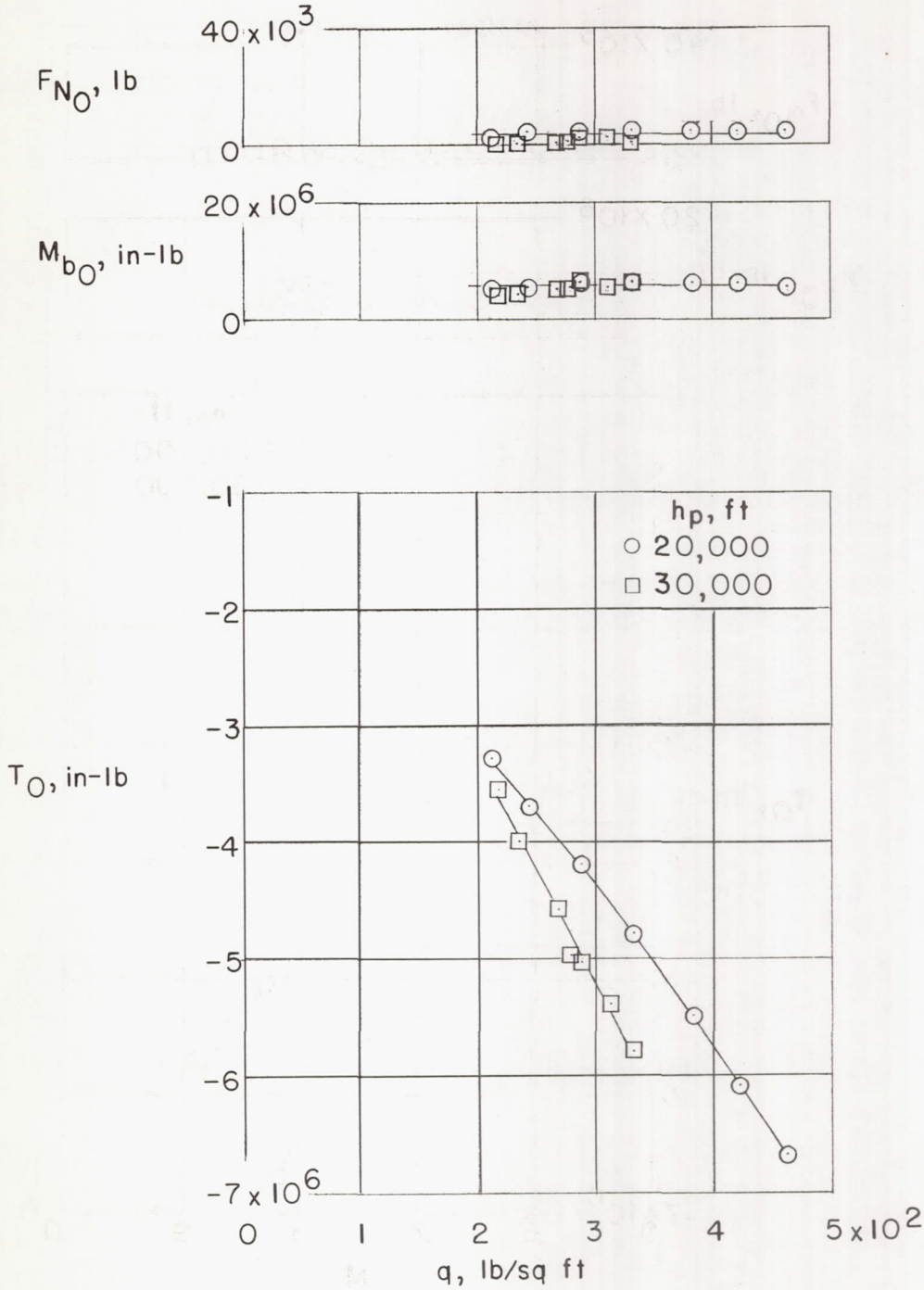

(b) Dynamic pressure.

Figure 10.- Concluded.

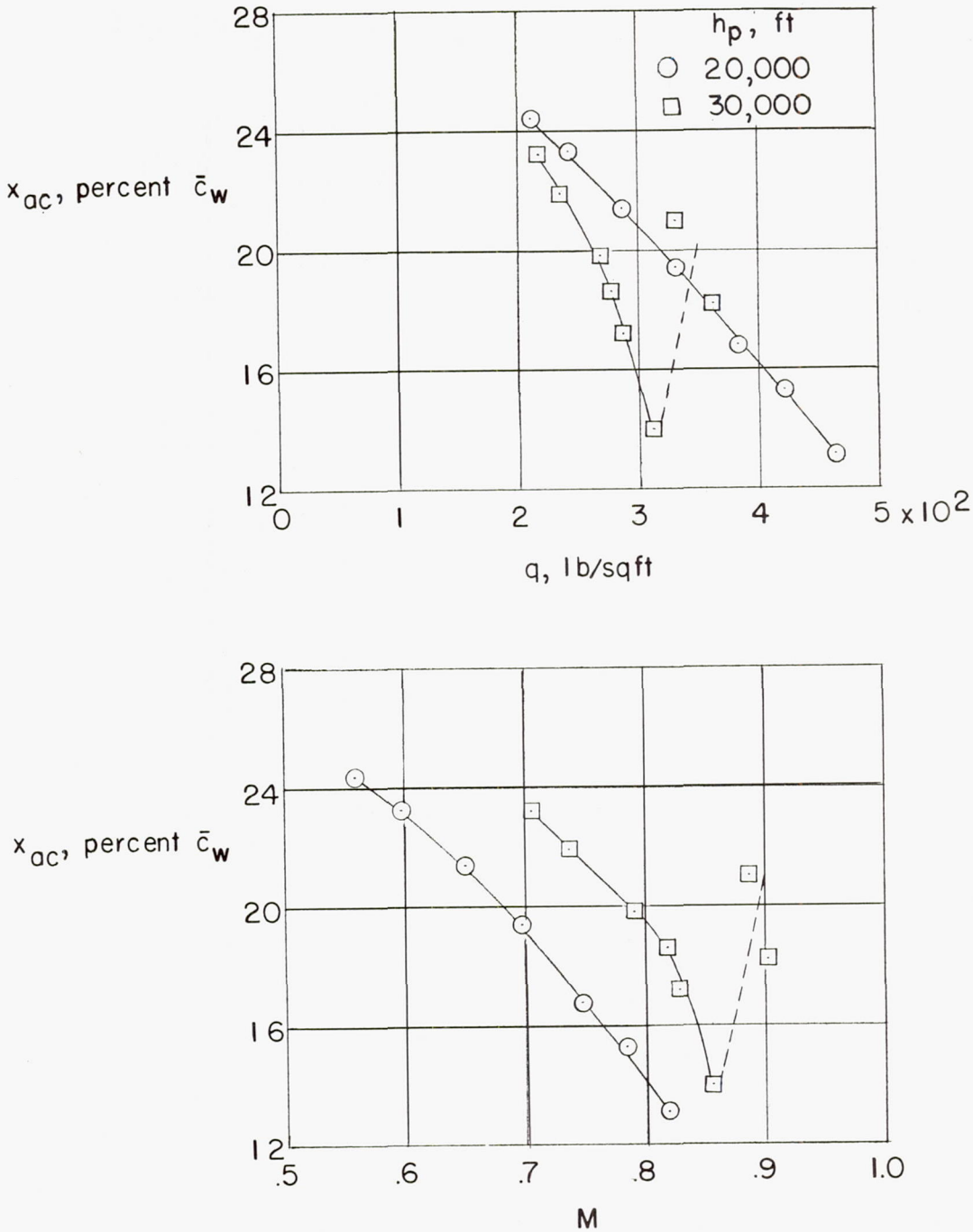

(a) Aerodynamic center.

Figure 11.- Variation with Mach number and dynamic pressure of wing-panel aerodynamic center and wing-panel center of pressure of additional air load.

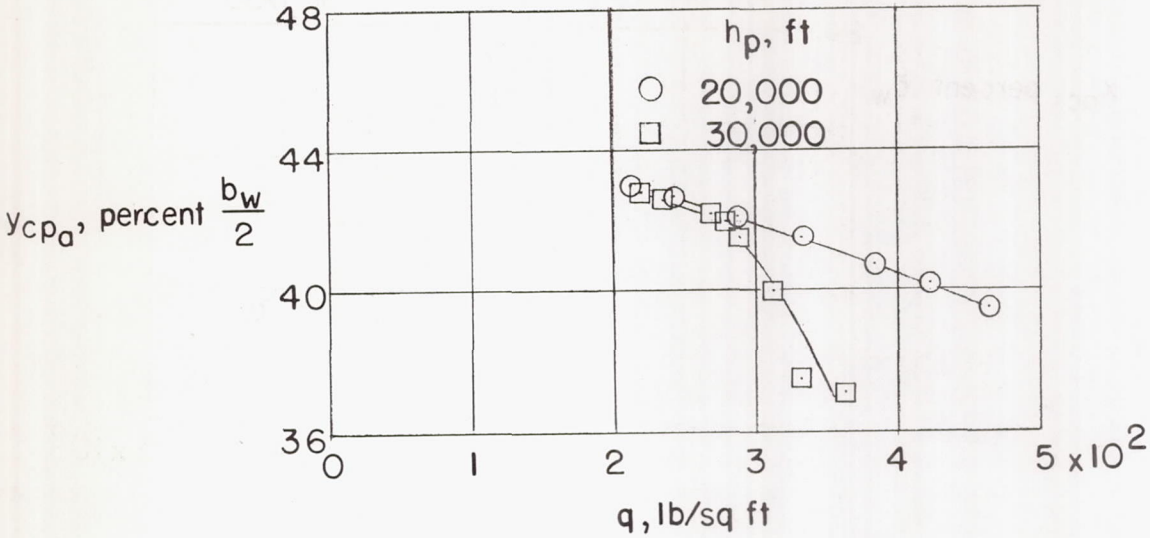

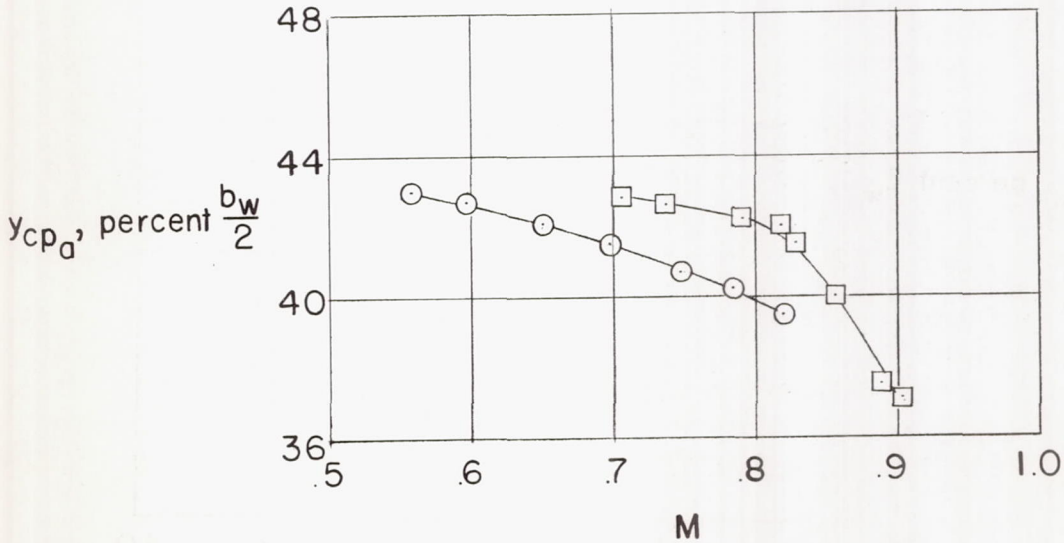

(b) Center of pressure.

Figure 11.- Concluded.

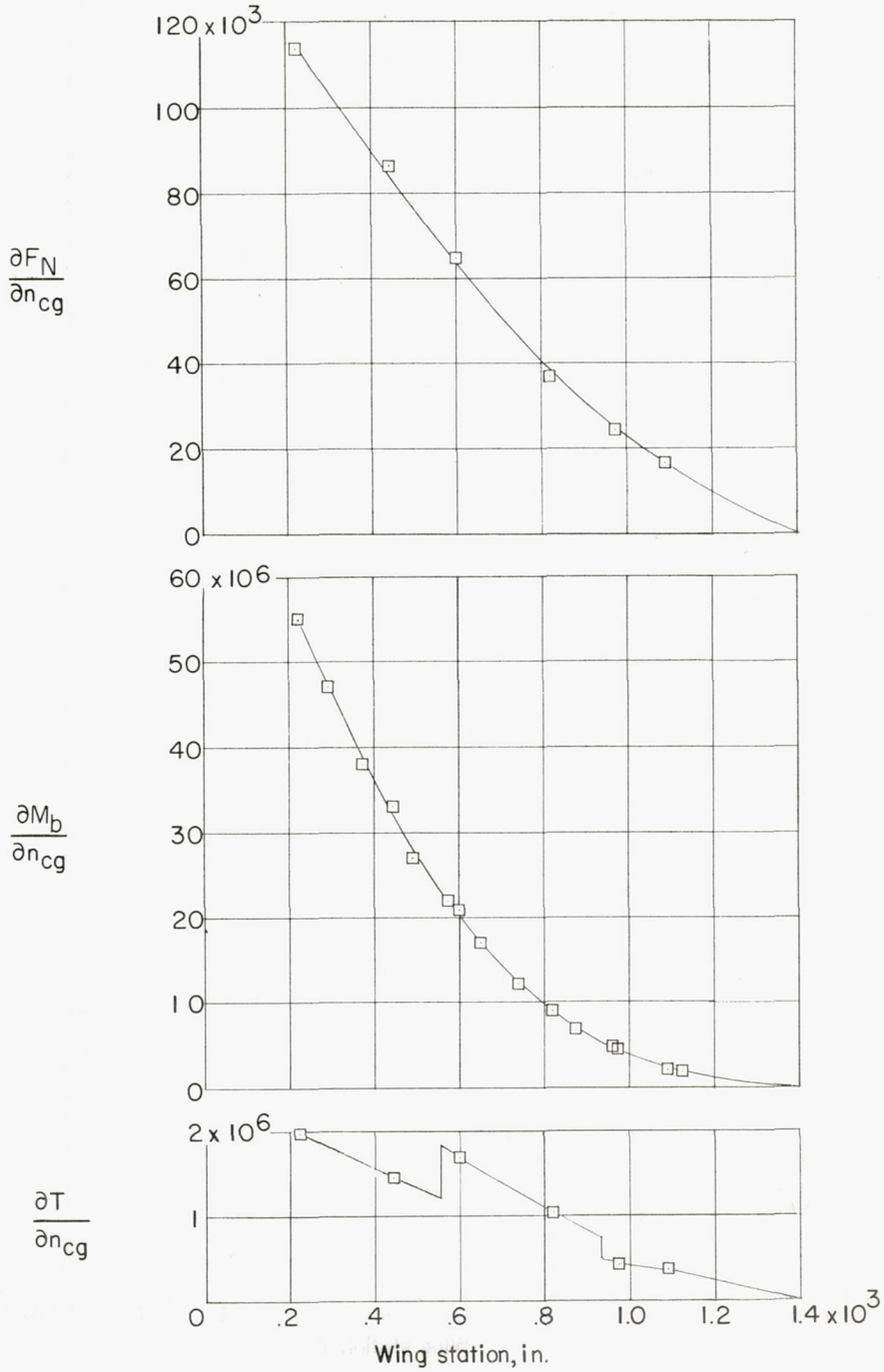

(a) M = 0.70; W = 291,000 pounds.

Figure 12.- Measured wing-span load distributions per unit normal-load factor at various Mach numbers. h_p = 30,000 feet.

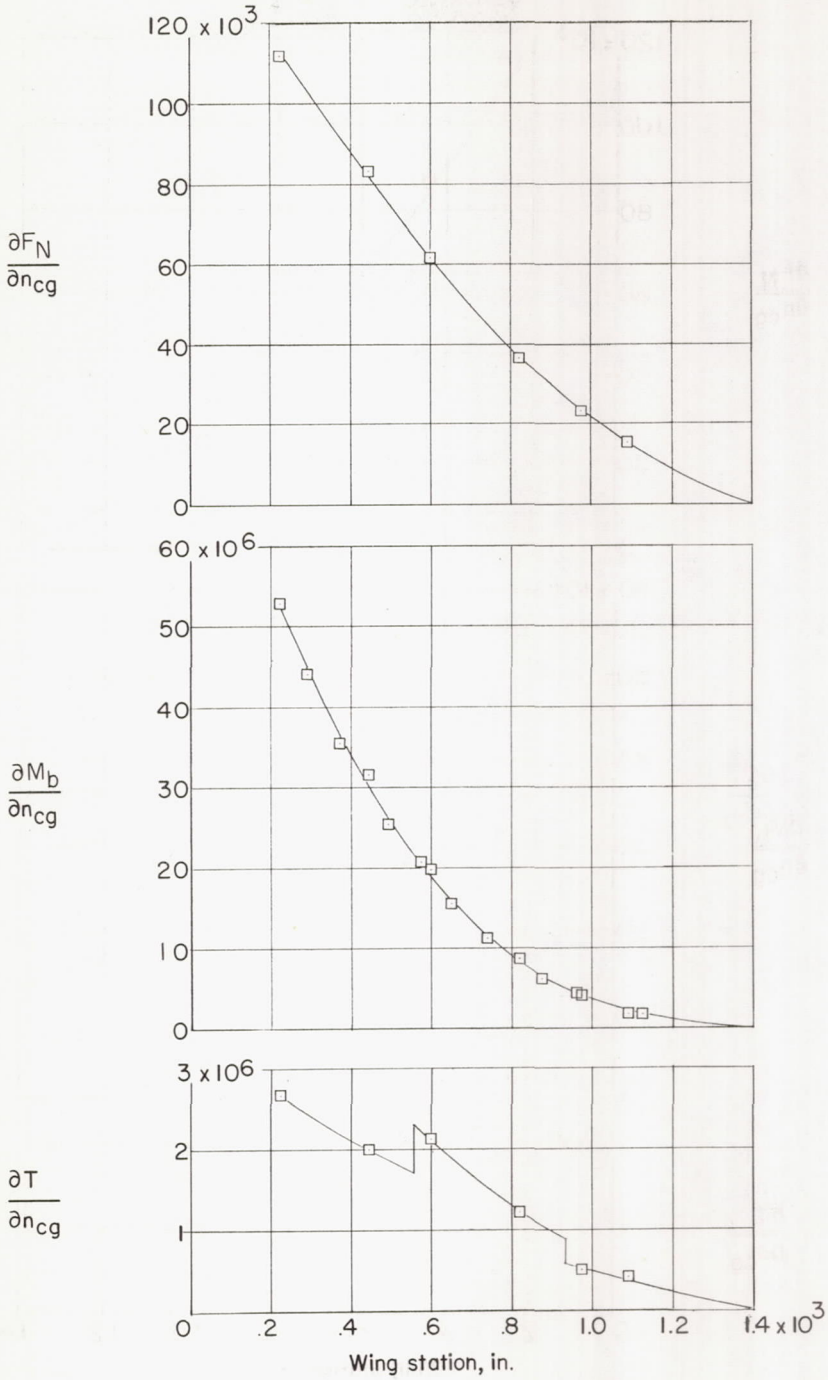

(b) M = 0.82; W = 288,700 pounds.

Figure 12.- Continued.

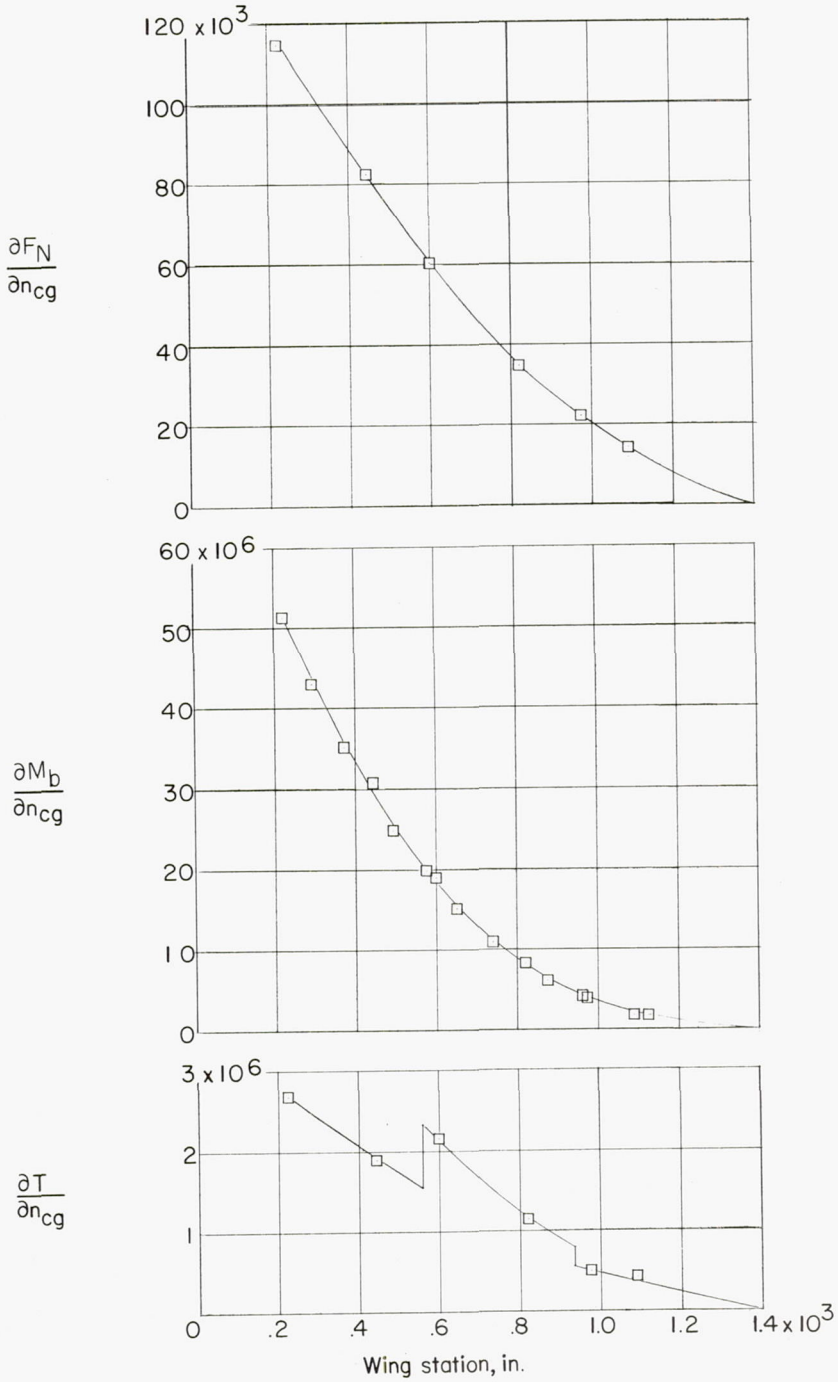

(c) M = 0.86; W = 286,600 pounds.

Figure 12.- Continued.

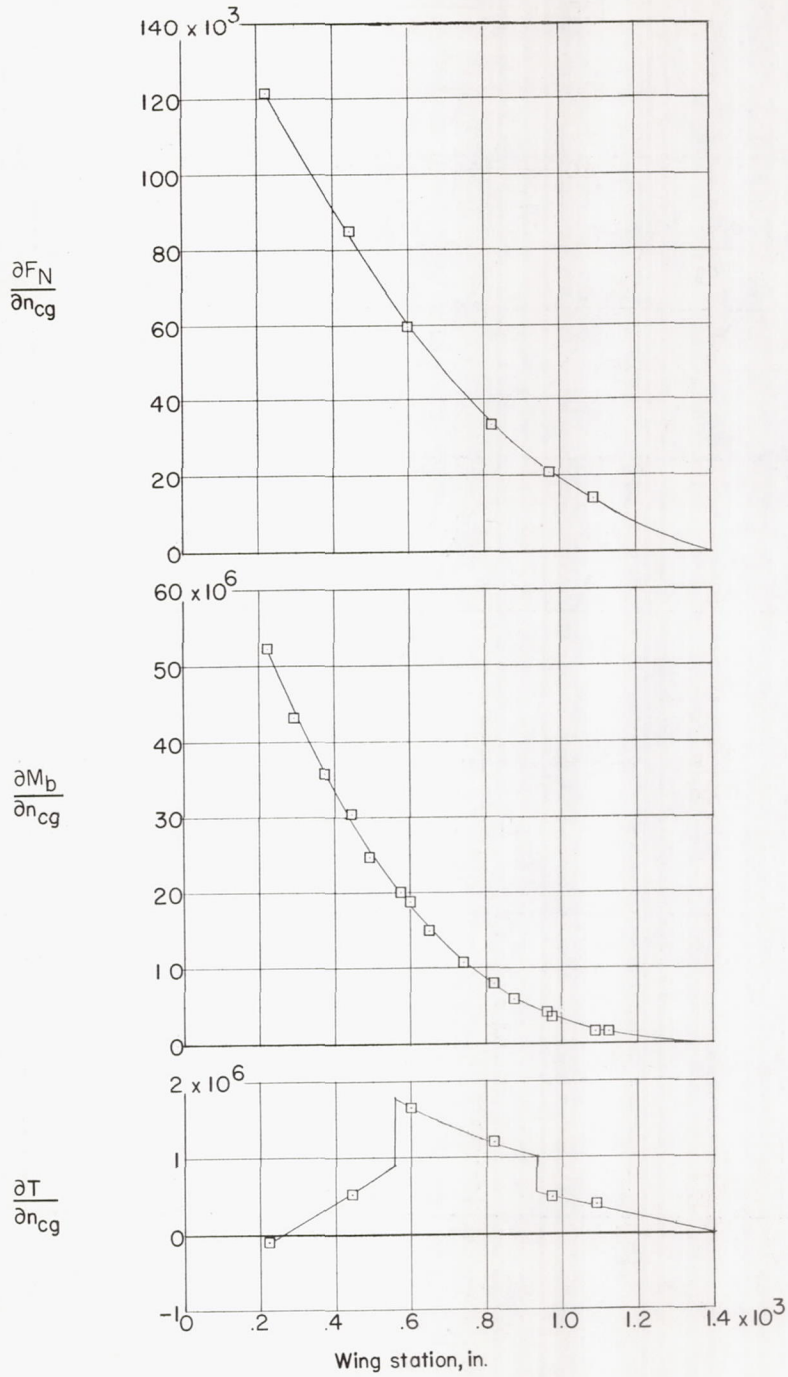

(d) M = 0.90; W = 285,400 pounds.

Figure 12.- Concluded.

CONFIDENTIAL

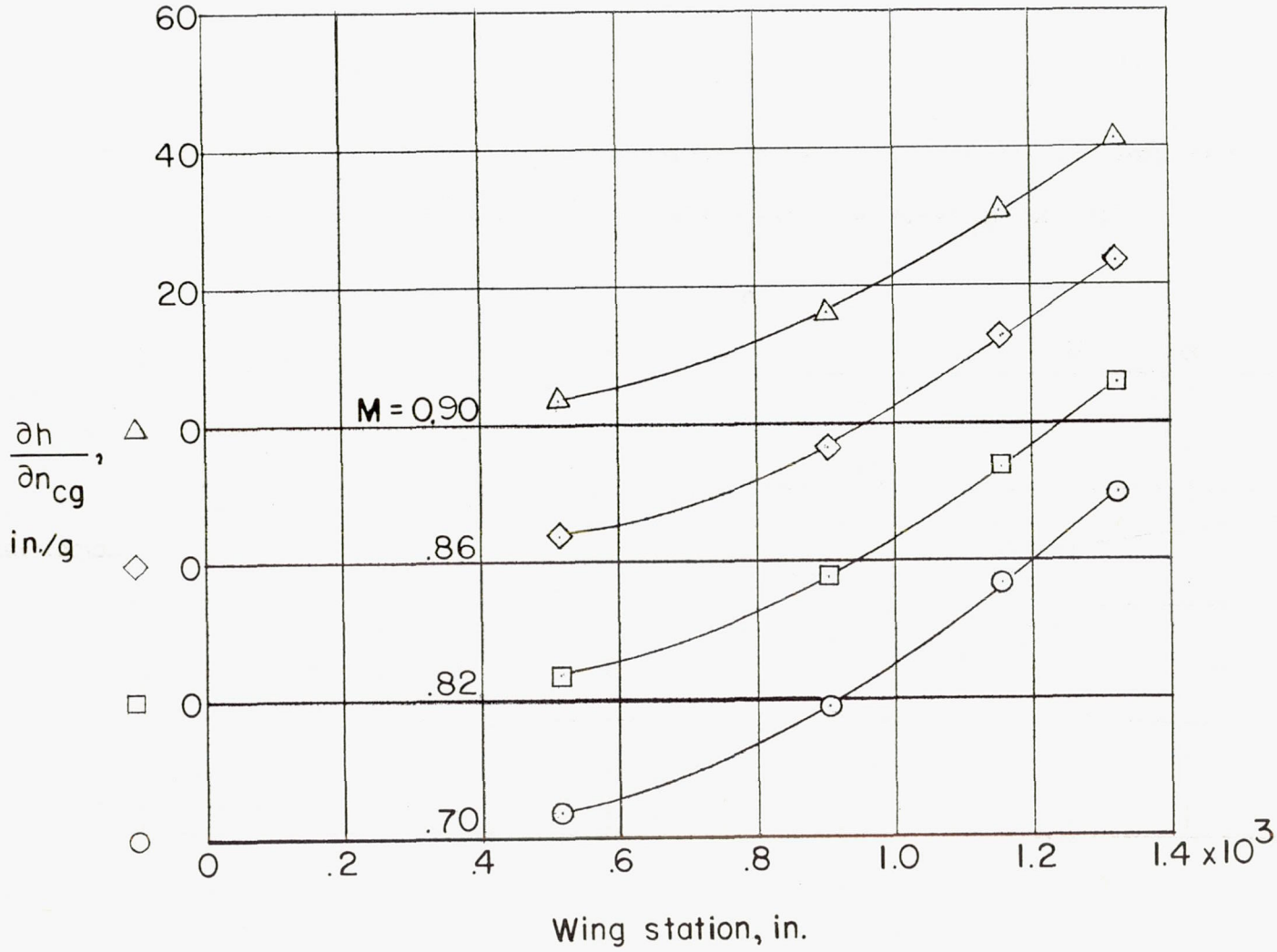

Figure 13.- Measured wing deflections per unit normal-load factor at various Mach numbers. h_p = 30,000 feet.

CONFIDENTIAL

CONFIDENTIAL

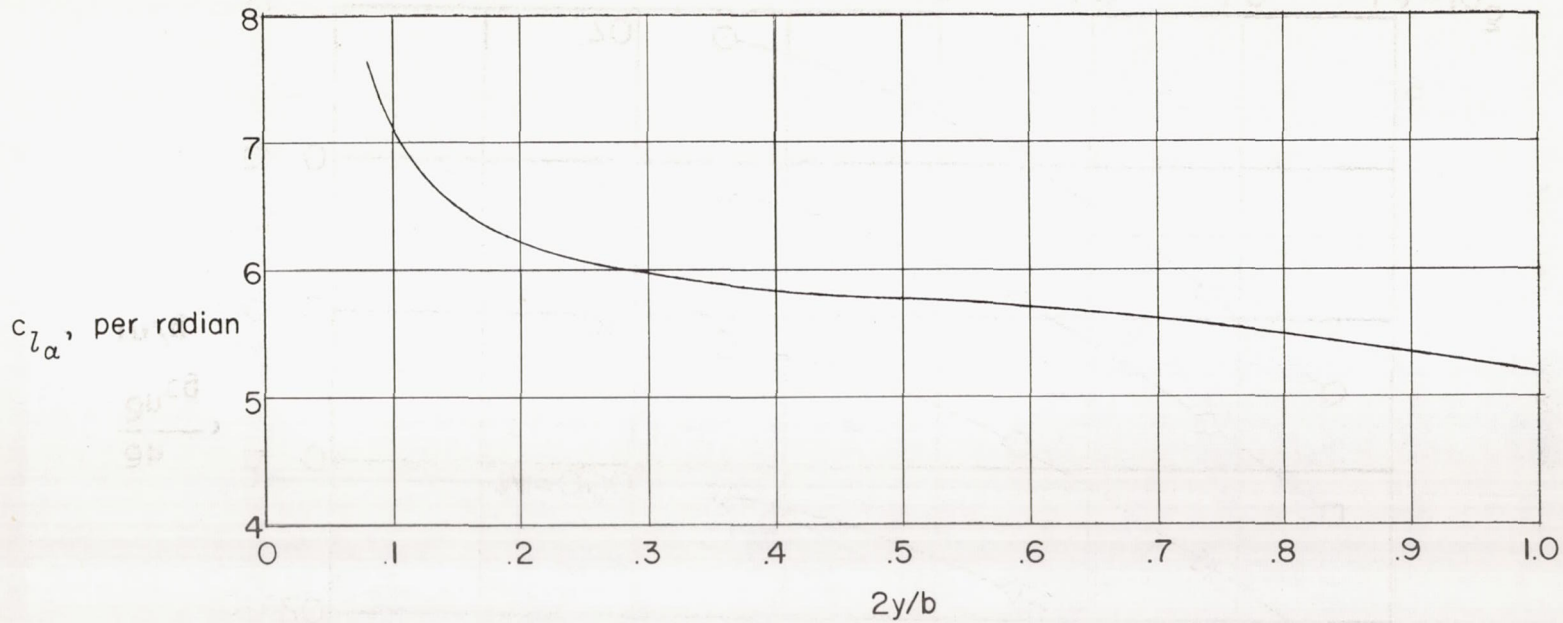

(a) Spanwise distribution of section lift-curve slope at M = 0.

Figure 14.- Structural and aerodynamic parameters used in air-load calculations.

CONFIDENTIAL

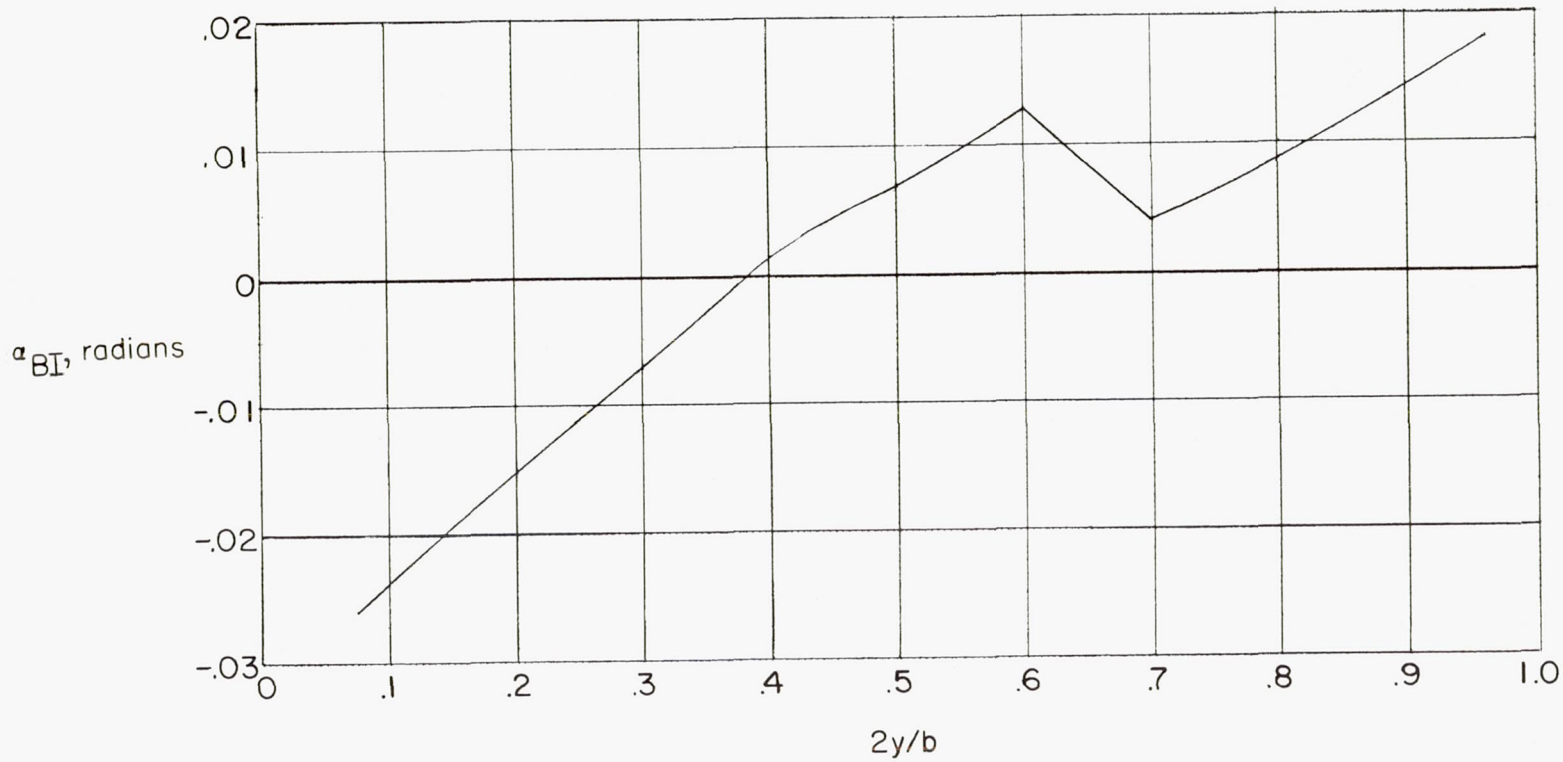

(b) Net zero lift line, including built-in twist and induced aerodynamic effects, α_{BI}.

Figure 14.- Continued.

[redacted]

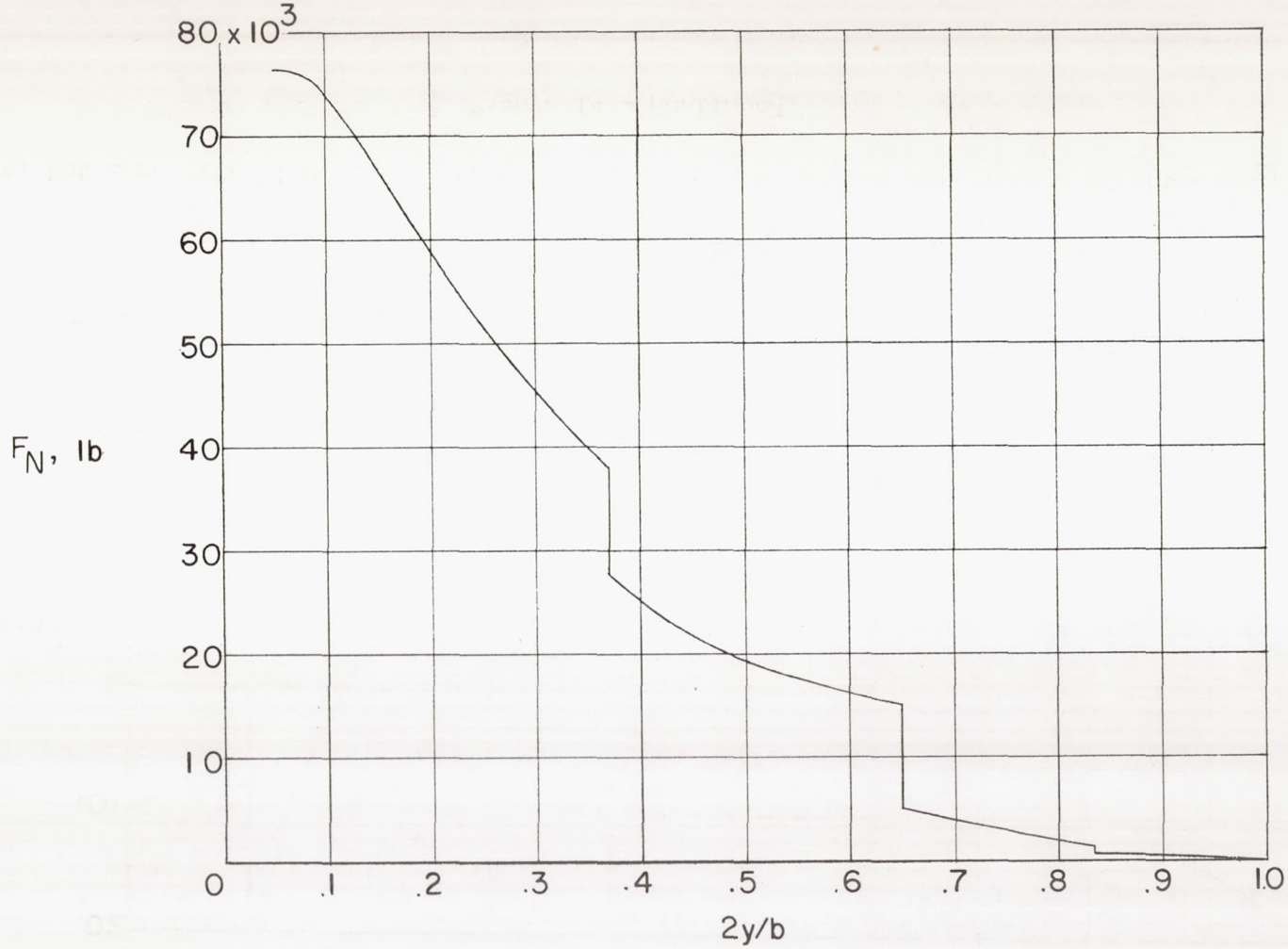

(c) Spanwise distribution of wing dead-weight shear.

Figure 14.- Continued.

[redacted]

CONFIDENTIAL

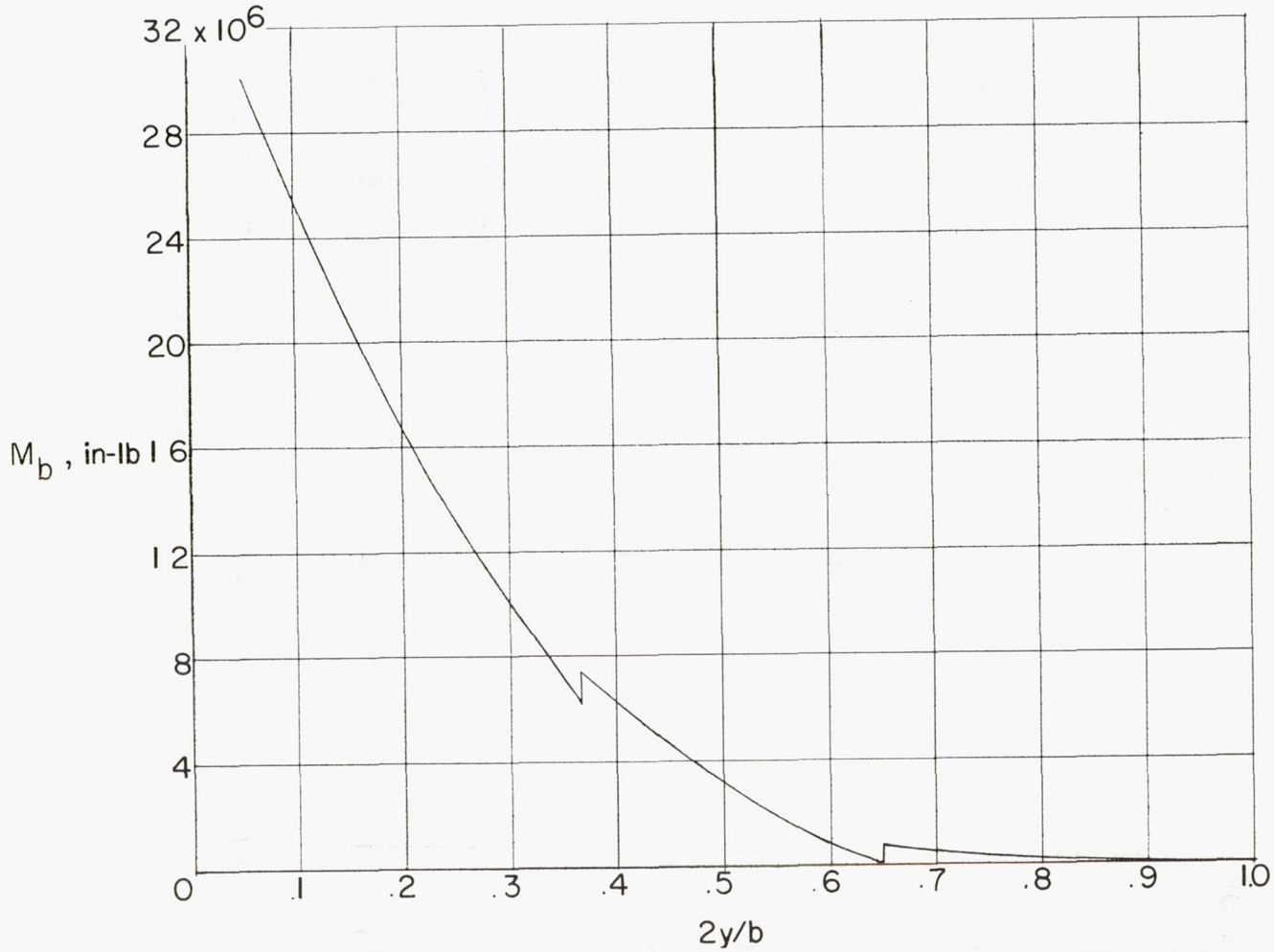

(d) Spanwise distribution of wing dead-weight bending moment.

Figure 14.- Continued.

CONFIDENTIAL

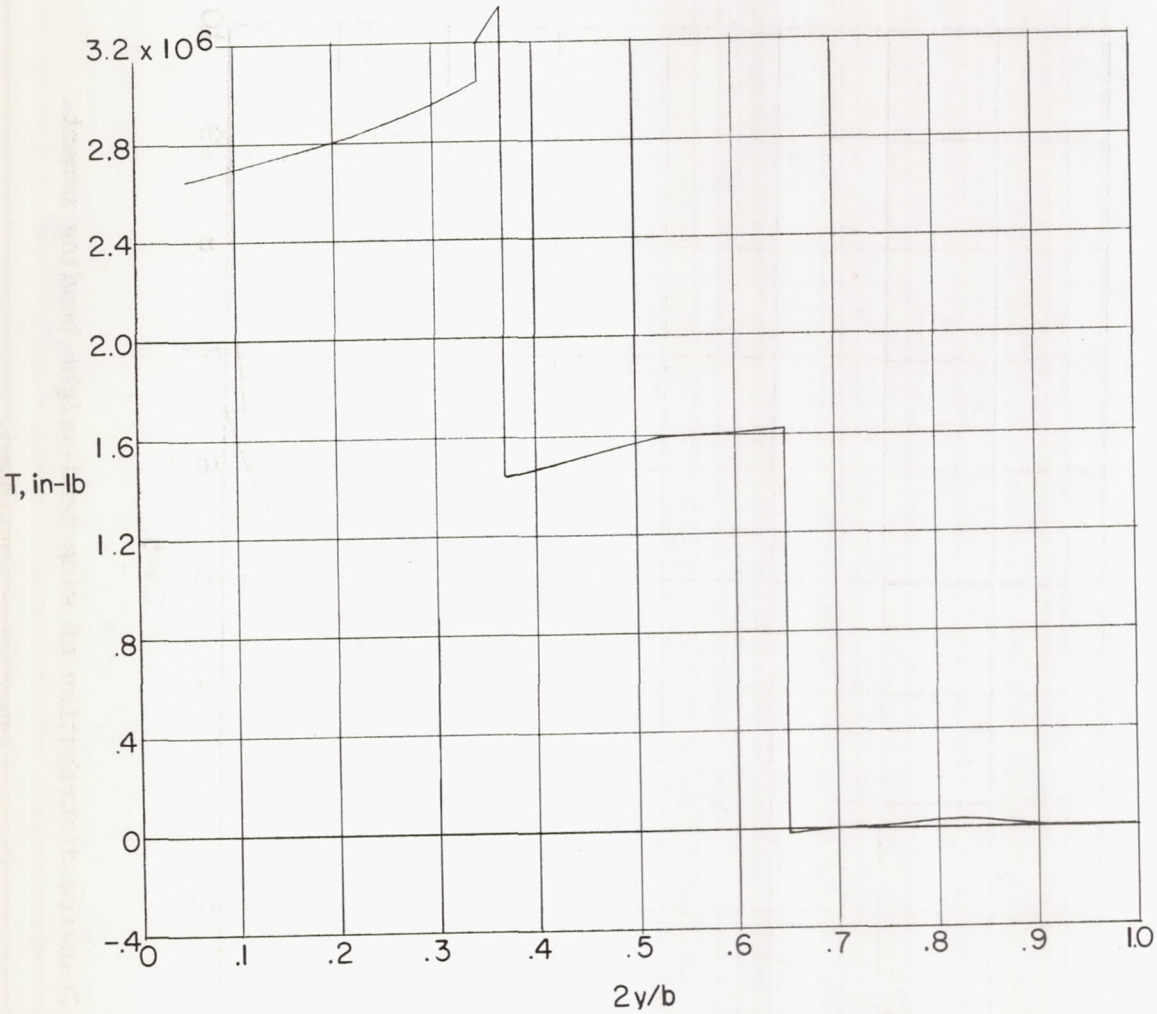

(e) Spanwise distribution of wing dead-weight torque.

Figure 14.- Continued.

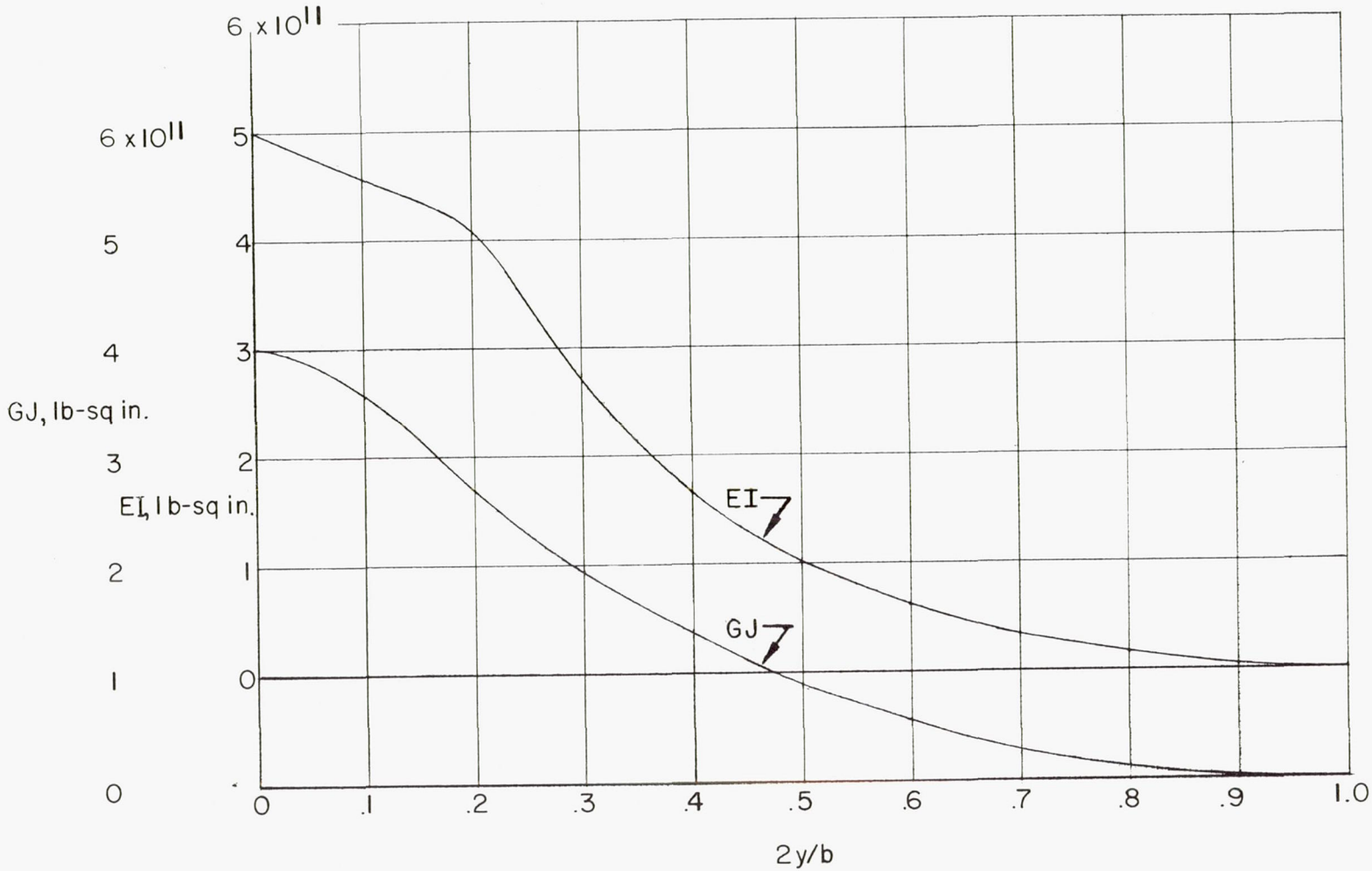

(f) Spanwise distribution of wing bending and torsional stiffness.

Figure 14.- Concluded.

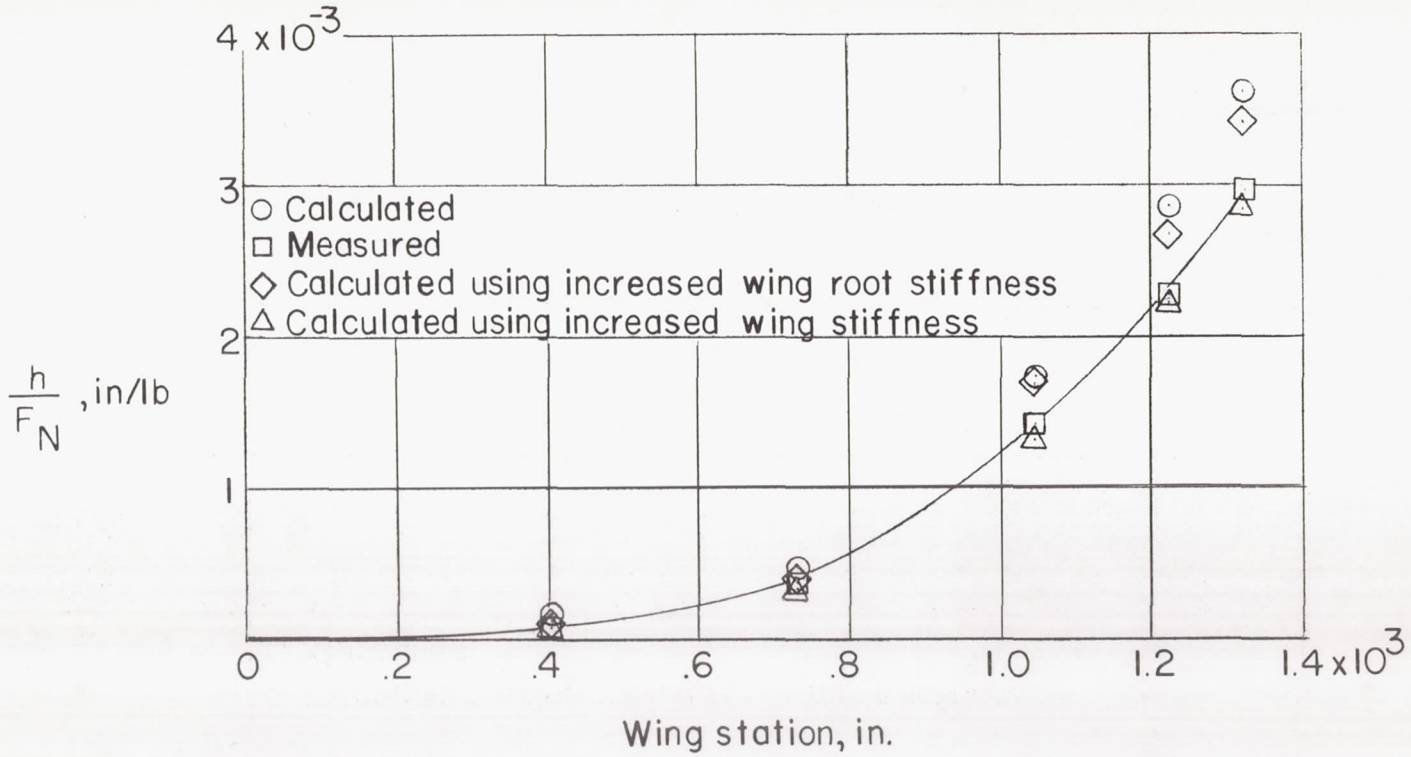

Figure 15.- Comparison of measured and calculated wing deflection at wing station 1325 per pound of applied load at various wing stations during static ground loading.

CONFIDENTIAL

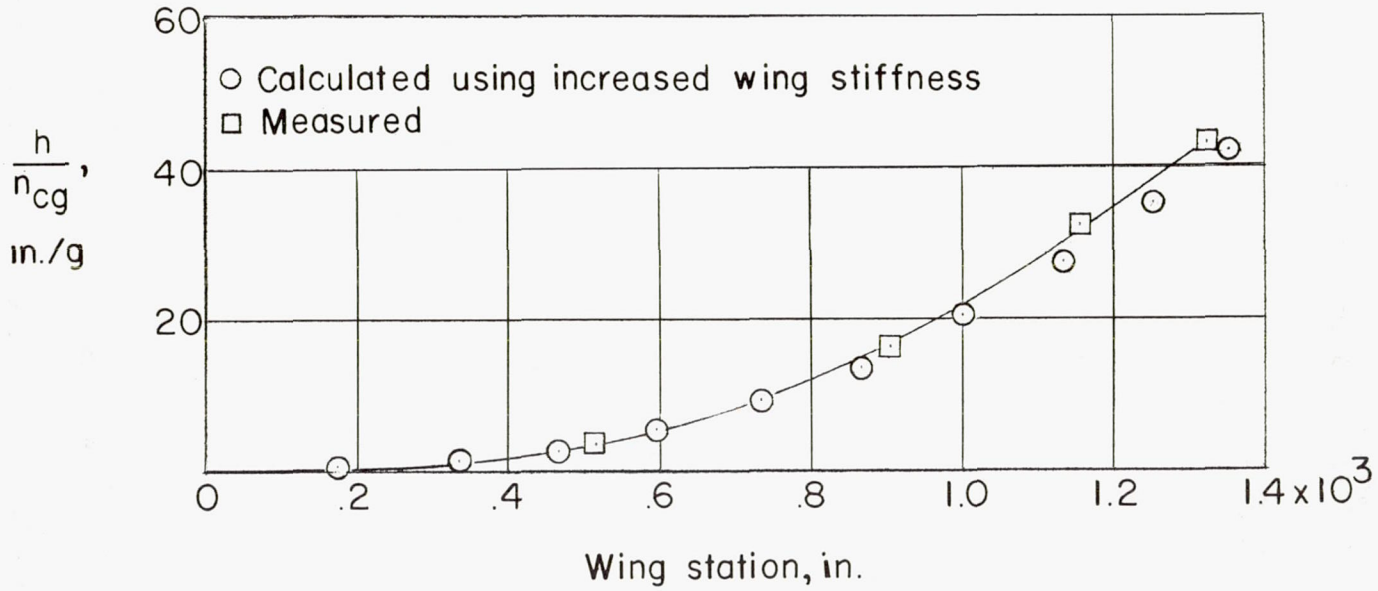

Figure 16.- Comparison of measured and calculated wing deflection using an increased value of wing stiffness. $M \approx 0.86$; $h_p = 30{,}000$ feet.

CONFIDENTIAL

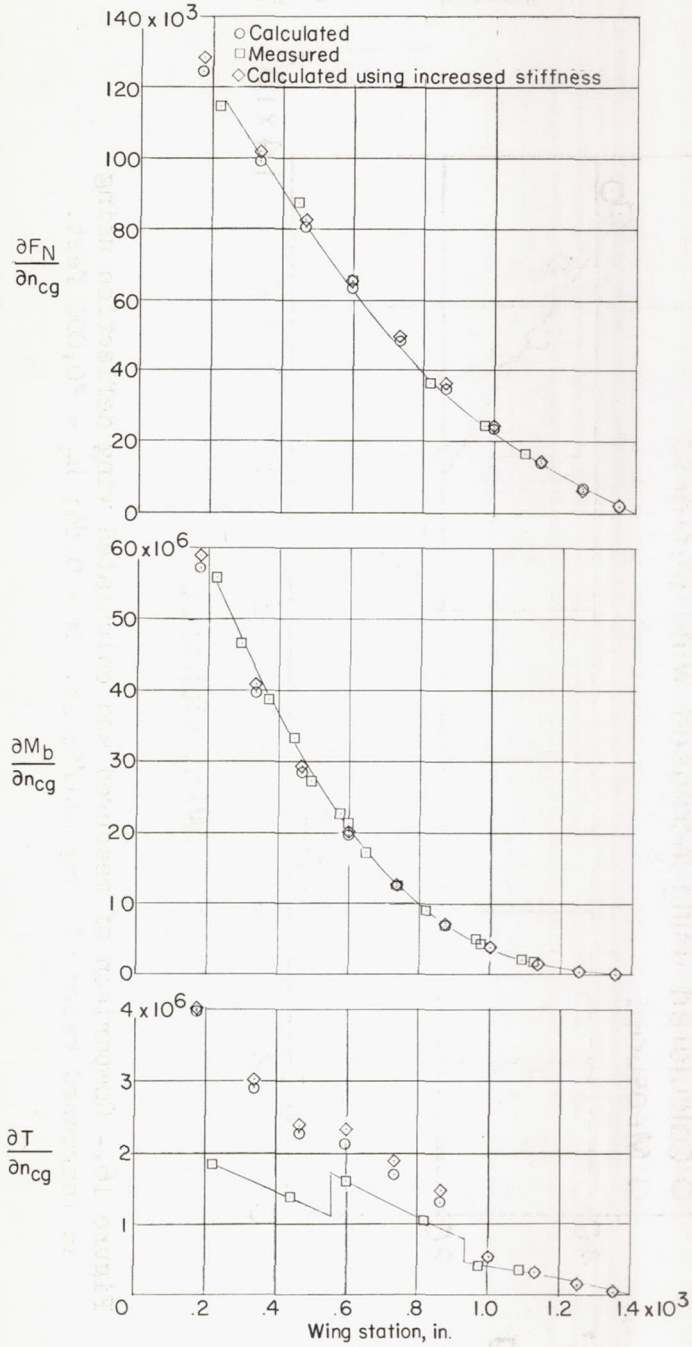

(a) M = 0.56; h_p = 20,000 feet; W = 295,400 pounds.

Figure 17.- Comparison of measured and calculated span-load distributions per unit normal-load factor.

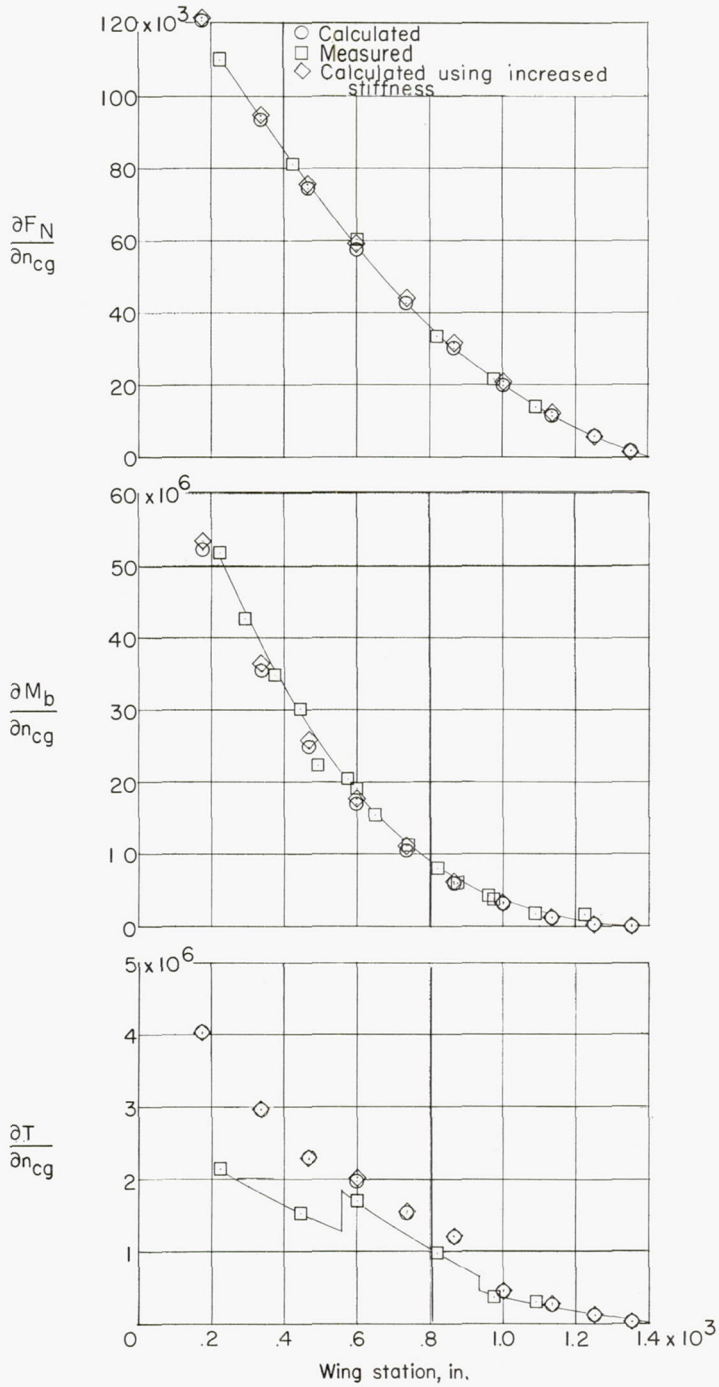

(b) M = 0.70; h_p = 20,000 feet; W = 291,600 pounds.

Figure 17.- Continued.

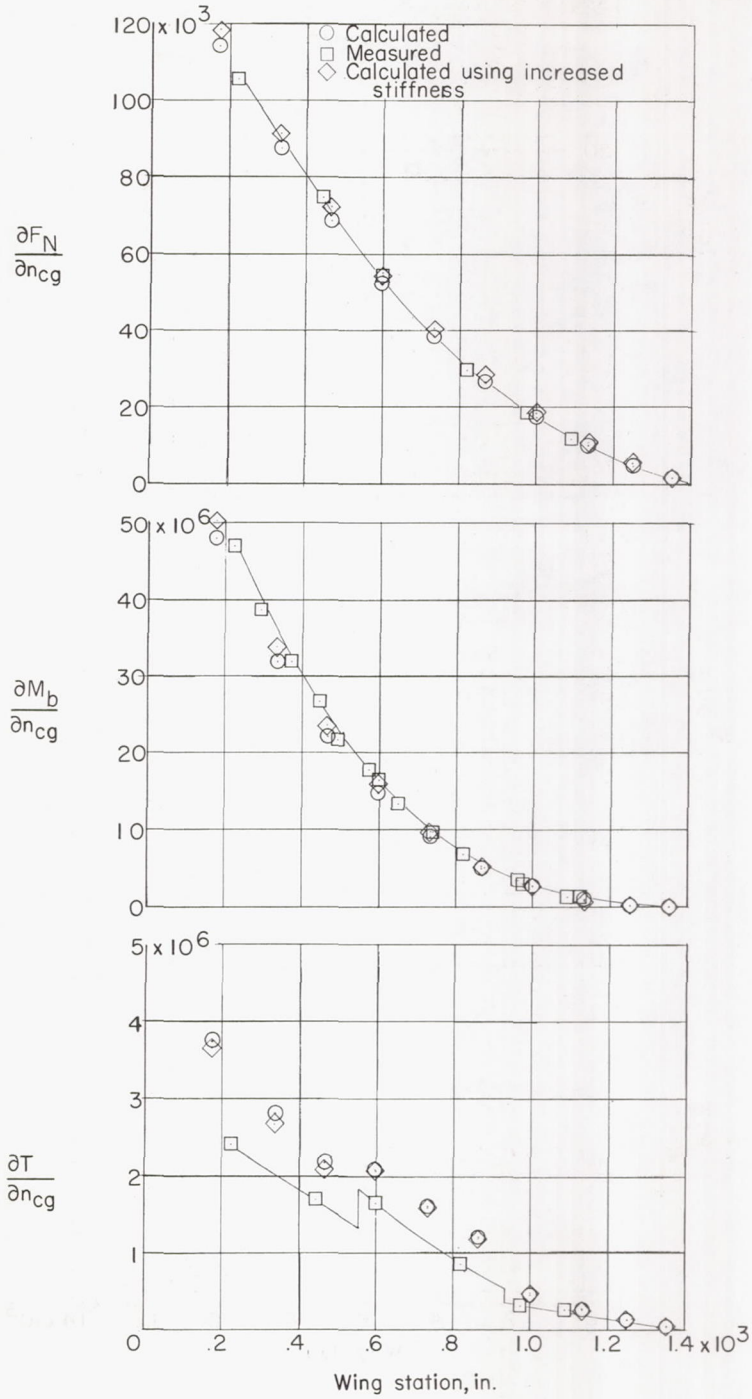

(c) M = 0.82; h_p = 20,000 feet; W = 286,300 pounds.

Figure 17.- Continued.

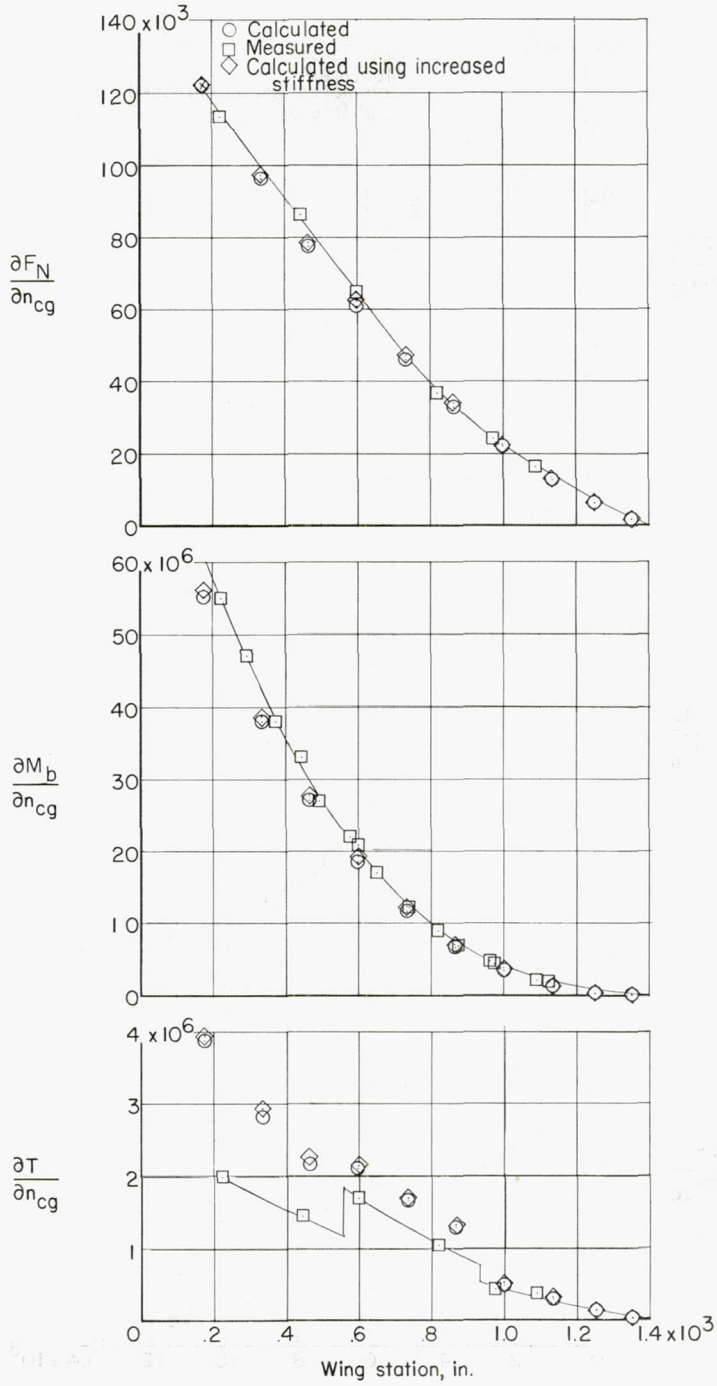

(d) M = 0.70; h_p = 30,000 feet; W = 291,000 pounds.

Figure 17.- Continued.

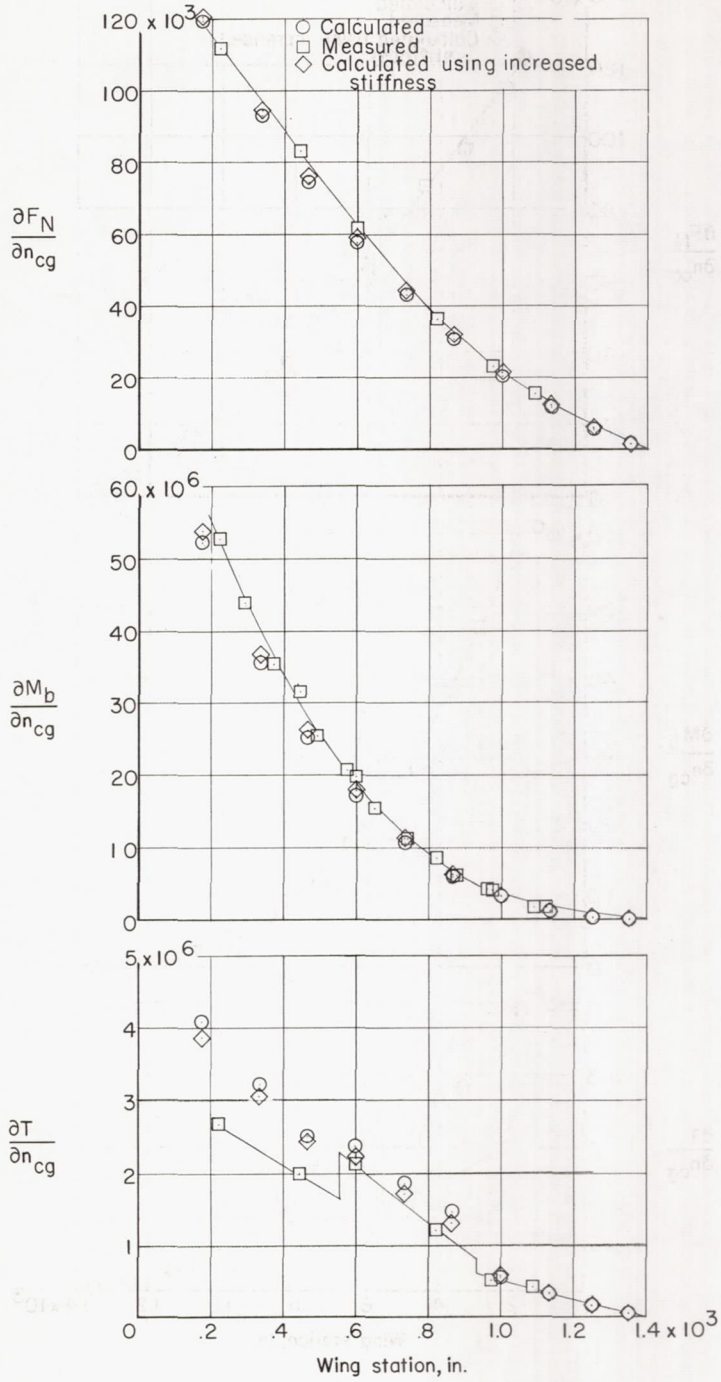

(e) M = 0.82; h_p = 30,000 feet; W = 288,700 pounds.

Figure 17.- Continued.

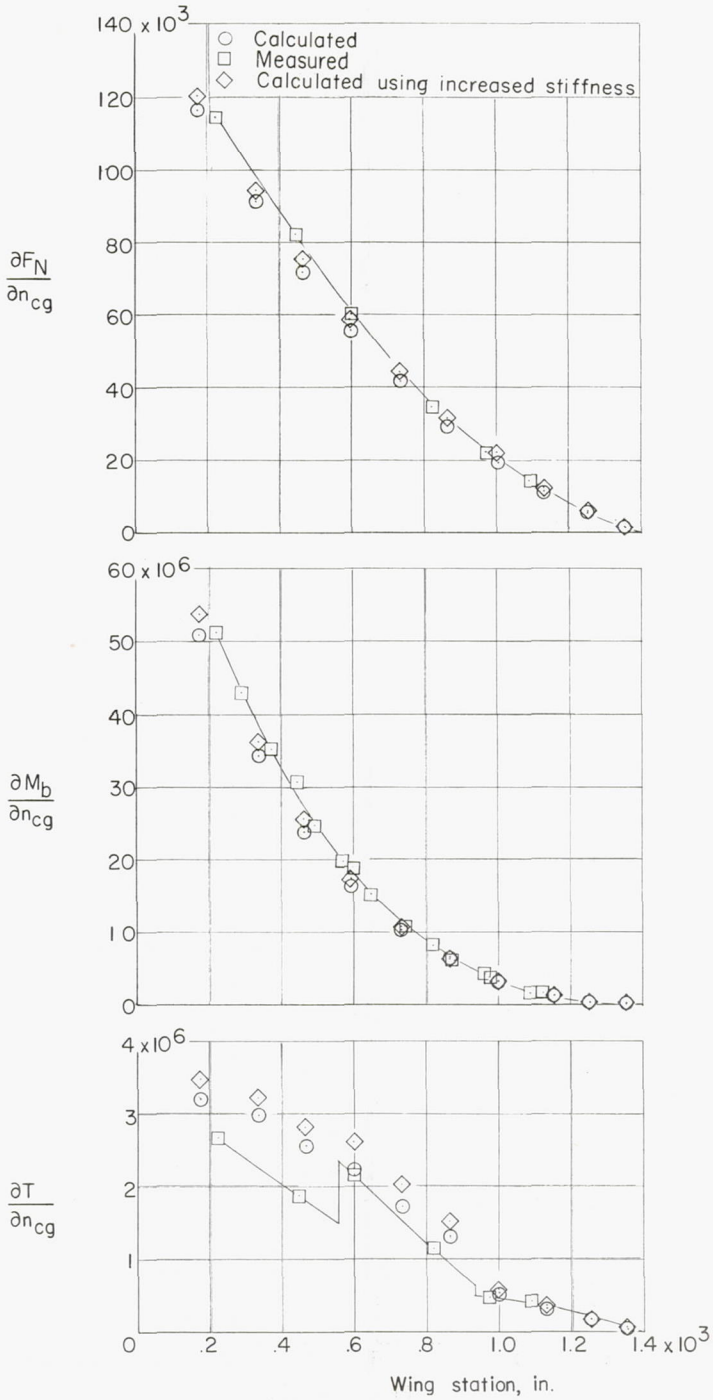

(f) M = 0.86; h_p = 30,000 feet; W = 286,600 pounds.

Figure 17.- Continued.

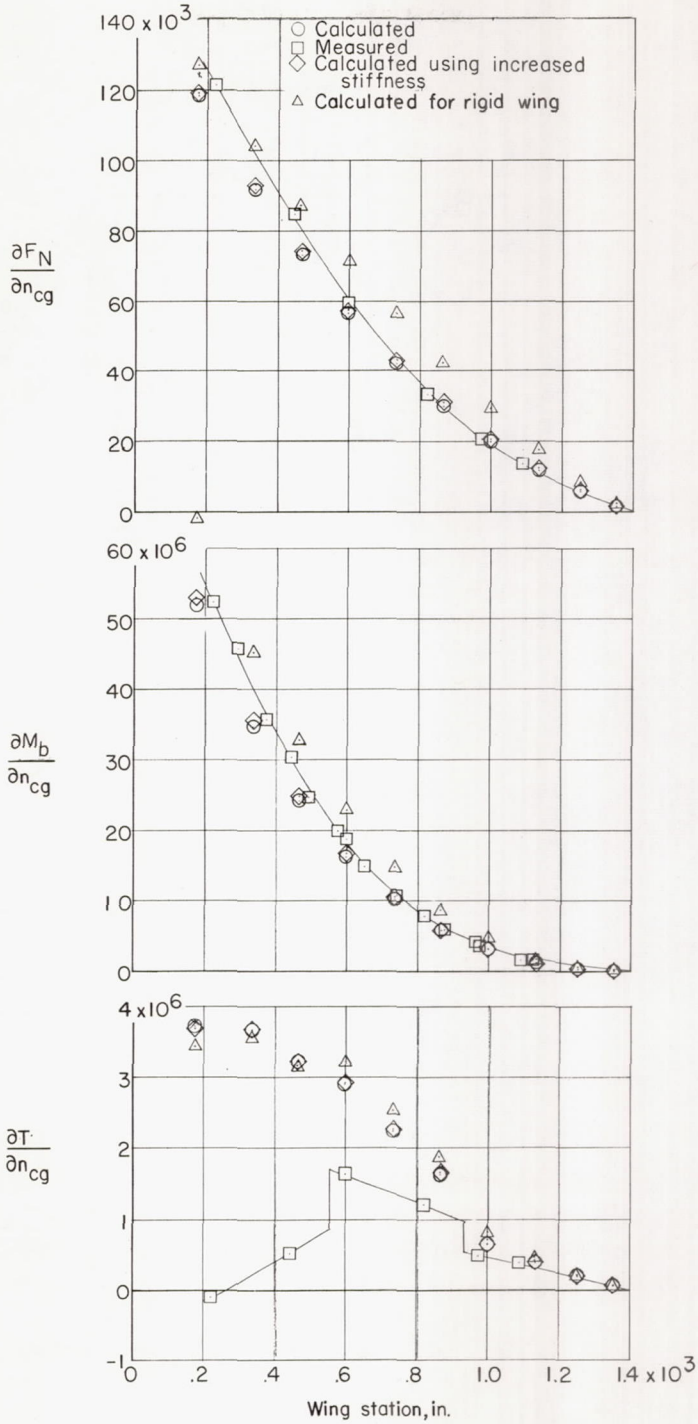

(g) M = 0.90; h_p = 30,000 feet; W = 285,400 pounds.

Figure 17.- Concluded.

NACA - Langley Field, Va.

[redacted]

[redacted]